bioRxiv preprint doi: https://doi.org/10.1101/2020.02.06.937839; this version posted March 14, 2020. The copyright holder for this preprint (which was not certified by peer review) is the author/funder. All rights reserved. No reuse allowed without permission.

Targeting OCA-B/Pou2af1 blocks type-1 diabetes and reduces infiltration of activated, islet-reactive T cells

Heejoo Kim[1,2], Jelena Perovanovic[1,2], Arvind Shakya[1,2,¶], Zuolian Shen[1,2], Cody N. German[1,2], Andrea Ibarra[1,2], Jillian L. Jafek[1,2], Nai-Pin Lin[3], Brian D. Evavold[1], Danny H.-C. Chou[3], Peter E. Jensen[1], Xiao He[1], and Dean Tantin[1,2,*]

[1]Department of Pathology, University of Utah School of Medicine, Salt Lake City, UT 84112, U.S.A.
[2]Huntsman Cancer Institute, University of Utah School of Medicine, Salt Lake City, UT 84112, U.S.A.
[3]Department of Biochemistry, University of Utah School of Medicine, Salt Lake City, UT 84112, U.S.A.

[*]Corresponding authors: Dean Tantin, Department of Pathology, University of Utah School of Medicine, Salt Lake City, UT 84112. E-mail address: dean.tantin@path.utah.edu

[¶]Current address: Celgene, Inc., San Diego, CA 92121

Running title: OCA-B in T1D

Manuscript data:

Characters in title (including spaces): 108
Words in abstract: 262
Character count (including spaces): 80,467
Total main figures: 7
Total main tables: 0

bioRxiv preprint doi: https://doi.org/10.1101/2020.02.06.937839; this version posted March 14, 2020. The copyright holder for this preprint (which was not certified by peer review) is the author/funder. All rights reserved. No reuse allowed without permission.

Abstract

Autoimmune therapies aim to inhibit autoreactivity while preserving normal immune function. The transcriptional coregulator OCA-B, also known as Bob.1/OBF-1 (gene symbol *Pou2af1*) is induced in stimulated naïve CD4$^+$ T cells, where it docks with transcription factor Oct1 to regulate genes such as *Il2* and *Ifng*. OCA-B promotes expression of these targets in cases of repeated antigen exposure, a necessary feature of autoimmunity. Polymorphisms in *Ocab* itself and binding sites for Oct1/OCA-B complexes are associated with multiple forms of autoimmunity including autoimmune (type-1) diabetes. We hypothesized that T cell-specific OCA-B deletion would protect mice from type-1 diabetes, and that pharmacologic OCA-B inhibition would provide similar protection. We developed an *Ocab* conditional allele and backcrossed it onto a diabetes-prone NOD/ShiLtJ strain background. T cell-specific OCA-B loss protected mice from spontaneous T1D. Protection was associated with reduced pancreatic T cell and macrophage infiltration and reduced proinflammatory cytokine expression. We profiled prediabetic pancreatic lymph nodes and islets by single-cell RNA sequencing and T cell receptor clonotype analysis. Although lymph nodes showed minimal differences, in the islets CD8$^+$ T cell specificities associated with diabetes pathogenesis failed to emerge in OCA-B deficient activated/memory cells. In contrast, CD4$^+$ clones associated with diabetes were present, but only in anergic cells. The protective effect of OCA-B loss was diminished, or even eliminated, using monoclonal models with high affinity to artificial or neoantigens. Rationally-designed membrane-penetrating OCA-B peptide inhibitors normalized glucose levels, and reduced T cell infiltration and proinflammatory cytokine expression in newly-diabetic NOD mice. Together, the results indicate that OCA-B is a potent autoimmune regulator and a promising target for pharmacologic inhibition.

bioRxiv preprint doi: https://doi.org/10.1101/2020.02.06.937839; this version posted March 14, 2020. The copyright holder for this preprint (which was not certified by peer review) is the author/funder. All rights reserved. No reuse allowed without permission.

Introduction

Type 1 Diabetes (T1D) is an autoimmune disease in which the host immune system is directed towards antigens associated with pancreatic beta cells[1, 2]. Pathologically, T1D is characterized by insulitis, beta cell destruction and inability to produce insulin. The main treatment for T1D, life-long insulin therapy, treats symptoms but not cause. The development of new T1D treatments is limited by an incomplete understanding of disease mechanisms[3]. Beta cell regeneration is a promising line of therapy, but still requires methods to specifically block T1D autoimmunity. An ideal method of therapy would be to capture patients early in the disease course and block autoimmunity while keeping normal immune function intact. Such a therapy would spare remaining beta cell function.

In $CD4^+$ T cells, the transcription factor Oct1 and its cofactor OCA-B regulate a set of ~150 target genes, including *Il2*, *Ifng* and *Csf2* (*Gmcsf*)[4]. Upon T cell activation, many of these targets are activated by pathways that converge on transcription factors such as NF-AT, AP-1 and NF-κB. Factors like NF-AT can be thought of as the primary on/off switches for these genes, and drugs that block NF-AT activation effectively block their expression. Such drugs have utility in many contexts, but also have drawbacks including global dampening of immune function and side effects due to expression in other tissues. In contrast, Oct1 and OCA-B insulate silent but previously activated target genes against stable repression. Loss of either protein does not affect $CD4^+$ T cell responses to stimulation in vitro or primary infection in mice[4, 5], but causes large defects in target gene expression upon secondary stimulation in vitro and defective $CD4^+$ memory T cell formation and recall responses in vivo[4, 6]. In addition, OCA-B expression is largely confined to lymphocytes. OCA-B is silent in thymocytes and naïve $CD4^+$ T cells, but is induced and stably expressed after sustained antigen stimulation[4]. Once expressed, OCA-B recruits the histone lysine demethylase Jmjd1a/Jhdm2a/Kdm3a to Oct1 at target loci, where it locally removes inhibitory H3K9me2 chromatin marks that would otherwise promote repressive chromatin environments[4, 6]. OCA-B also potentiates polarization of activated helper T cells towards the Th17 phenotype, among the most pro-inflammatory helper T cell subsets[7].

Persistent antigen exposure is a common property of autoimmune responses. Among profiled $CD4^+$ T cell subsets, OCA-B levels are elevated in both central memory cells and pancreas-infiltrating, islet-reactive cells (http://www.immgen.org/databrowser/index.html). Both Oct1 and OCA-B are highly conserved to humans, and genome-wide association studies identify Oct1/OCA-B binding site polymorphisms that confer predisposition to a variety of human autoimmune diseases including T1D, multiple sclerosis, lupus, inflammatory bowel disease and rheumatoid arthritis[8, 9, 10, 11, 12, 13, 14]. Other

bioRxiv preprint doi: https://doi.org/10.1101/2020.02.06.937839; this version posted March 14, 2020. The copyright holder for this preprint (which was not certified by peer review) is the author/funder. All rights reserved. No reuse allowed without permission.

84 studies implicate polymorphisms at the *Ocab* (*Pou2af1*) locus itself in different forms autoimmunity[15,
85 16]. We therefore hypothesized that targeting OCA-B would inhibit diabetogenic T cell responses.
86 Here, we generate a T cell conditional mouse model of OCA-B deficiency. We show that
87 OCA-B ablation protects animals from spontaneous, polyclonal T1D. Protection was associated with
88 reduced T cell infiltration and proinflammatory cytokine expression. Conditional OCA-B deletion
89 maintained normal pancreatic lymph node cell populations, numbers, gene expression and TCR
90 clonality. In contrast, significant alterations in specific TCR clones were present in the pancreatic islets
91 of OCA-B T cell conditional mice. Protection from OCA-B loss varied among different TCR
92 transgenic and monoclonal antigen models, and was weakest using synthetic antigens and monoclonal
93 transplant models. Protection was stronger, but still incomplete, using a spontaneous CD8 TCR
94 transgenic model. Using a rational-design approach, we developed membrane-penetrating OCA-B
95 peptide inhibitors that are efficacious in vitro and in mice. Collectively, the results indicate that OCA-
96 B is a potent and pharmacologically accessible autoimmune regulator.

bioRxiv preprint doi: https://doi.org/10.1101/2020.02.06.937839; this version posted March 14, 2020. The copyright holder for this preprint (which was not certified by peer review) is the author/funder. All rights reserved. No reuse allowed without permission.

Results

Generation of an *Ocab* conditional allele and NOD backcrossing. We generated a conditional *Ocab* (*Pou2af1*) mouse allele using embryonic stem cells provided by the knockout mouse project (KOMP) repository. Deletion of the *LoxP* sites is predicted to create a null allele by disrupting the first three exons (Fig. 1a). Breeding chimeric mice resulted in germline transmission and a founder mouse (Fig. 1B, lane 2) that was crossed to a FLP deleter mouse strain (FLP^{Rosa26}) to remove the reporter cassette and create a floxed conditional allele (Fig. 1a and b, lane 3). Intercrossing these mice generated homozygous *fl/fl* mice (Fig. 1b, lane 4). The mice were crossed to germline Cre deleter strain (Cre^{Rosa26}) to generate null (Δ) alleles (lanes 5 and 6). As expected, homozygous *fl/fl* mice produce normal amounts of both p34 and p35 OCA-B protein isoforms (Supplementary Fig. 1a, lane 6), while no protein of either isoform is present in germline-deleted Δ/Δ spleens (lanes 7-8). These results indicate that the *fl* allele is OCA-B sufficient and the Cre-deleted allele is a null. Crossing the *fl* allele onto a Cre^{CD4} driver, which deletes in both CD4 and CD8 compartments, resulted in efficient deletion in splenic T cells (Fig. 1b). These findings indicate that this allele represents a robust system in which to study OCA-B function in T cells.

The *Ocab* (*Pou2af1*) conditional allele was generated on a C57BL/6 background. To test the prediction that OCA-B expression in T cells promotes T1D emergence, we conducted speed congenic backcrosses to the NOD strain background. This method allows spontaneous diabetes to be produced rapidly by screening and selecting for 13 microsatellite and SNP markers associated with NOD autoimmune susceptibility[17]. Backcrossing is facilitated by the fact that *Ocab* is located on mouse chromosome 9 and is not nearby any of the *Idd* loci. Following these markers with specific primer pairs (Supplementary Table 1), we produced backcrossed animals with all 13 markers (Supplementary Fig. 1b) that recapitulate spontaneous autoimmunity (not shown). For example, *Idd1*, which maps to the MHC region[18], converted to the homozygous NOD allele after 2 backcross generations (Supplementary Fig. 1B, lane 3), whereas *Idd13*, which maps near beta-2-microglobulin[19] became NOD homozygous after 4 generations (lane 4). Genotyping identified this fourth-generation backcrossed animal as having all 13 microsatellite markers and the *Ocab* conditional allele (Supplementary Fig. 1c, #122). This founder animal was crossed to NOD.Cre^{CD4} and the floxed allele homozygosed in order to delete OCA-B in T cells to assess the effects on T1D. Similar NOD backcrosses, conducted using *Ocab* null mice[20], resulted in OCA-B germline-deficient NOD mice (data not shown). As with the original C57BL/6 OCA-B germline knockout[20], all alleles were viable and fertile with no obvious health issues.

bioRxiv preprint doi: https://doi.org/10.1101/2020.02.06.937839; this version posted March 14, 2020. The copyright holder for this preprint (which was not certified by peer review) is the author/funder. All rights reserved. No reuse allowed without permission.

Normal baseline T cell status in NOD mice lacking OCA-B. To study broad effects of T cell-specific OCA-B loss on T cell function, we performed single-cell RNA sequencing (scRNAseq) and TCR clonotype analysis using $CD3^+$ T cells isolated from PLNs of pre-diabetic 8 week-old female NOD.*Ocab*$^{fl/fl}$Cre^{CD4} or NOD.*Ocab*$^{fl/fl}$ littermate controls. For each group cells from three animals were combined for microfluidics and subsequent sequencing. T cells were isolated from PLNs of three animals in each group and combined for analysis. ~6000 knockout and ~3000 control cells were identified in this analysis, most of which comprise naïve CD4 and CD8 cells (Supplementary Fig. 2a, pink and orange), and regulatory T cells (Tregs, green). There was also a small population of activated $CD4^+$+$CD8^+$ cells (green), presumably in the process of exiting the lymph nodes. Other than a small decrease in the percentage of activated $CD4^+$+$CD8^+$ cells (4.4 vs 6.1%), few differences in the populations were observed. None of these populations expressed measurable amounts of *Ocab* (*Pou2af1*) mRNA (not shown), however *Pou2af1* is expressed at low levels in T cells making it difficult capture by scRNAseq. In addition, few changes in gene expression were identified, and the great majority of these were not of immunological interest (Supplementary Fig. 2b, Supplementary Table 2). We also determined TCR repertoires in these T cell populations, identifying few changes as a whole (Supplementary Fig. 2c). However, specific sub-populations did show changes in TCR utilization. For example, NOD $CD8^+$ T cells expressing *Trbv13-3* (Vβ8.1) display reactivity to islet-specific glucose-6-phosphatase catalytic subunit related protein (IGRP) and are associated with T1D[21]. Although this clone was unchanged across the entire population of T cells (Supplementary Fig. 2c), it was over-represented in the effector $CD8^+$ population (Supplementary Fig. 2d). In contrast, other TCR clonotypes such as *Trbv13-1*, *Trbv13-2*, *Trbv1* and *Trbv15* were unchanged (not shown). This result was confirmed with flow cytometric staining of $CD8^+$ T cells using Vβ8.1 antibodies (Supplementary Fig. 2e). This change was coupled with a decrease the presence of this particular clone in pancreatic islets (below). These results indicate that OCA-B loss does not result in gross changes PLN T cell repertoire or status, but results in lymph node retention of potentially autoreactive clones.

NOD mice lacking OCA-B are protected from T1D. T1D onset in NOD mice is spontaneous and acute[22]. To test the impact of OCA-B loss in T cells on spontaneous T1D, we compared incidence in in female NOD.*Ocab*$^{fl/fl}$Cre^{CD4} mice, and controls lacking the Cre^{CD4} driver. Glucose was monitored 2-3 times per week. Using a 250 mg/dL blood glucose cutoff, approximately 60% of *Ocab*$^{fl/fl}$ control mice manifested spontaneous diabetes by 24 weeks of age, while no *Ocab*$^{fl/fl}$Cre^{CD4} mice became diabetic

bioRxiv preprint doi: https://doi.org/10.1101/2020.02.06.937839; this version posted March 14, 2020. The copyright holder for this preprint (which was not certified by peer review) is the author/funder. All rights reserved. No reuse allowed without permission.

(Fig. 1d). Blood glucose was stable in *Ocab*$^{fl/fl}$Cre^{CD4} females but began to spike in control mice beginning at week 16, rising to an average of >300 mg/dL by 24 weeks (Fig. 1e). Similar results were observed using female whole-body knockout NOD.*Ocab*$^{-/-}$ compared to *Ocab*$^{+/+}$ littermate controls. While ~80% of control females developed T1D within 24 weeks after birth, only ~20% of NOD.*Ocab*$^{\Delta/\Delta}$ females did so (Fig. 1f). Cumulatively, the results show that OCA-B expression in T cells is critical for T1D pathogenesis in NOD mice.

NOD.*Ocab* conditional mice have fewer islet macrophages and IFNγ–expressing cytotoxic T cells, and more Tregs. We sacrificed *Ocab*$^{fl/fl}$Cre^{CD4} female mice and controls at 8 and 24 weeks, and determined the frequencies of immune cells in the pacreata. We observed more T cells in the pancreata of OCA-B deficient mice (not shown). This result is understandable because the control mice have annihilated their pool of beta cells, resulting in lack of antigen. We also studied pancreatic macrophages in these mice. Islet infiltration of F4/80$^+$CD11b$^+$ macrophages is critical for NOD T1D pathogenesis both in spontaneous and adoptive transfer T1D models[23, 24]. CCL1 expressed in diabetogenic CD4 T cells is known to recruit CCR8-expressing macrophages[25]. Interestingly, OCA-B deletion in stimulated, rested and re-stimulated CD4$^+$ T cells decreases *Ccl1* mRNA expression compared to controls (Supplementary Table 3). We therefore hypothesized that OCA-B expression in T cells is important for macrophage islet infiltration. Despite the fact that antigen and greater numbers of T cells were present, we observed 5-fold fewer macrophages in 24 week-old NOD.*Ocab*$^{fl/fl}$Cre^{CD4} islets (Fig. 2a,b). In contrast, macrophage numbers were unaffected by T cell-specific OCA-B loss in pre-diabetic (8 week) mice (Fig. 2a).

IFNγ is a direct OCA-B target gene[4] and a strong promoter of T1D. Levels of serum and pancreatic IFNγ gradually rise in young NOD mice, reaching maximum at diabetes onset[26]. Diabetogenic CD4$^+$ and CD8$^+$ T cells both express IFNγ in humans and NOD mice[27, 28, 29]. Therefore, we predicted that OCA-B loss would reduce islet IFNγ expression in CD4$^+$ and CD8$^+$ T cells. We compared IFNγ-expressing pancreatic CD4$^+$ and CD8$^+$ T cells in female NOD.*Ocab*$^{fl/fl}$Cre^{CD4} and littermate control mice lacking Cre^{CD4}. In 12 week-old prediabetic mice, CD8$^+$ T cell frequencies were significantly decreased (Fig. 2c), whereas CD4$^+$ T cells at the same timepoint were unchanged (data not shown). At the time of diabetes onset (16 weeks), proportionally fewer IFNγ-expressing CD8$^+$ T cells were present in *Ocab* conditional-deleted mice compared to controls (Fig. 2d).

CD4$^+$CD25^{HI}FoxP3$^+$ Tregs interfere with T1D development in NOD mice[30, 31]. Analysis of previously generated RNAseq datasets shows that naïve *Ocab* null CD4$^+$ T cells express 4-fold more

bioRxiv preprint doi: https://doi.org/10.1101/2020.02.06.937839; this version posted March 14, 2020. The copyright holder for this preprint (which was not certified by peer review) is the author/funder. All rights reserved. No reuse allowed without permission.

193 *Foxp3* mRNA compared to controls upon in vitro stimulation (Supplementary Table 3). To determine
194 whether the protection conferred by T cell conditional OCA-B is associated with changes in Tregs, we
195 analyzed pancreatic Treg frequencies, observing a trend towards more Tregs in pre-diabetic (8 week-
196 old) NOD.*Ocab*$^{fl/fl}$Cre^{CD4} mice compared to controls (Fig. 2e). Interestingly, there were no differences
197 late in disease course, at 16 or 24 weeks (data not shown).
198 If increased Treg numbers help mediate protection in NOD.*Ocab*$^{fl/fl}$Cre^{CD4} mice, then depletion
199 of these Tregs would be expected normalize T1D pathogenesis in knockout mice relative to controls.
200 Anti-CD25 antibody injection in neonatal NOD mice depletes Tregs (as well as activated T cells), and
201 accelerates T1D onset[32]. Surprisingly, we observed that anti-CD25 antibody-injected
202 NOD.*Ocab*$^{fl/fl}$Cre^{CD4} mice were still protected from T1D development relative to controls, though to a
203 lesser degree than in undepleted mice (Fig. 2f). These results support a conclusion that Tregs partly
204 contribute to the T1D protection in mice lacking OCA-B in their T cells.
205
206 **T cell-specific OCA-B deletion alters the islet-infiltrating TCR repertoire.** We performed
207 scRNAseq and TCR clonotype analysis similar to Supplementary Fig. 2, but using older (12 week) but
208 still pre-diabetic NOD.*Ocab*$^{fl/fl}$Cre^{CD4} or NOD.*Ocab*$^{fl/fl}$ littermate control female mice, and using total
209 CD45$^+$ cells isolated from pancreatic islets rather than PLNs. Cells were isolated from four animals per
210 group and combined for microfluidics and sequencing. After filtering, ~6200 knockout and ~3800
211 control cells were identified. Overlaying cell from both genotypes, we used their gene expression
212 profiles to definitively identify multiple cell lineages, including naïve CD4$^+$ + CD8$^+$ T cells,
213 memory/effector CD4$^+$ T cells, memory/effector CD8$^+$ T cells, B cells, macrophages and neutrophils
214 (Fig. 3a). The biggest relative change in populations was neutrophils, which decreased from 3.4 to
215 1.4% in conditional knockout islets (Fig. 3a). B cells were also decreased, albeit more slightly. These
216 changes were accompanied by an increase in the percentages of CD4$^+$ and CD8$^+$ T cells with naïve
217 phenotypes in conditional knockouts (31.7 vs. 25%). Like endpoint diabetic animals (Fig. 2a,b),
218 macrophage numbers were decreased but only slightly. Unlike PLNs, prediabetic islets showed
219 significant changes in gene expression between the two groups (Fig. 3b), the strongest of which
220 occurred in neutrophils (e.g., *Cxcl2*, down), memory/effector CD8$^+$ T cells (*Ccl4*, *Tcrg-v1*, *Itga*, down;
221 *Tcrbv1*, *Trav8n-2*, up), NK T cells (*Klra2*, *Lars2*, down) and γδT cells (*Gzma*, *Gzmb*, *Ccl5*, down).
222 We also profiled TCR clonality in pancreatic T cells. Across total T cells, few changes were
223 observed (Supplementary Fig. 3), however this was largely to do similar representation in the naïve T
224 cell pool. Isolating just antigen-experienced CD4$^+$ and CD8$^+$ effector + memory subpopulations

bioRxiv preprint doi: https://doi.org/10.1101/2020.02.06.937839; this version posted March 14, 2020. The copyright holder for this preprint (which was not certified by peer review) is the author/funder. All rights reserved. No reuse allowed without permission.

revealed sharp differences. For example, polyclonal NOD mice $CD8^+$ T cells expressing *Trbv13-3* (Vβ8.1) display reactivity to IGRP and are associated with T1D[21]. Relative to controls, this clonotype was under-represented in OCA-B deficient effector + memory $CD8^+$ cells (Fig. 3c, 20.9% vs 8.6%). Approximately half of these cells showed reactivity to $IGRP_{206-214}$ based on tetramer staining (data not shown). Based on this information, we repeated the clonotype analysis, but only using the effector + memory $CD8^+$ T cell cluster. Within this population, dominant TCR clonotypes used by conditional and control T cells were strikingly different (Fig. 3d). Clonotype 1 for example corresponds to a TCRα V8N-2 chain paired with TCRβ V1 or V15 and has not been associated with T1D. This clonotype was absent in control islets but represented >4% of OCA-B deficient islet $CD8^+$ effector + memory T cells (Fig. 3d). Clonotype 1 cells overlaid with both genotypes is shown in Fig. 3e. Clonotype 2 by contrast is associated with the T1D-associated Vβ13.3 β chain. This clonotype was strongly represented in controls (>3%) but absent from experimental effector + memory $CD8^+$ cells (Fig. 3d). In contrast to CD8-dominant TCR clonotypes, CD4-dominant TCRs associated with T1D were still present in knockouts, but associated with markers of anergy. For example, clonotype 4 (*Trav13-1/16N+Trbv15*) is associated with pro-diabetogenic, BDC-reactive $CD4^+$ T cells[33]. This clonotype was enriched in the OCA-B deficient effector + memory $CD4^+$ cells, but only in a CTLA4- and FR4-expressing sub-population (Fig. 3e). Cumulatively, these results indicate that OCA-B loss from T cells significantly skews the landscape of islet effector/memory-like T cells, in particular $CD8^+$ T cells, to an anti-diabetogenic phenotype.

Protection conferred by OCA-B loss is model-specific. T1D in NOD mice originates from defective negative selection in developing T cells, resulting in T cell autoreactivity. OCA-B is not expressed in thymocytes and OCA-B loss does not appear to affect T cell development[4]. Therefore, the protective effect of OCA-B loss in T cells likely arises from blunting pre-existing autoreactivity in the periphery. To test the hypothesis that OCA-B loss confers protection in simplified systems, we crossed OCA-B deficient mouse models employing TCR transgenes and model antigens.

Depleting Tregs and transferring remaining T cells from BDC2.5 TCR transgenic mice into NOD.Scid mice results in disease after approximately 10 d[34, 35]. We crossed the germline null *Ocab* allele to BDC2.5 mice to test the effect of OCA-B in this model. We transferred $CD4^+CD25^-$ T cells from germline $Ocab^{-/-}$ or $Ocab^{+/+}$ BDC2.5 mice into NOD.Scid recipients, monitoring diabetes emergence. Transplants from both $Ocab^{-/-}$ and control NOD.BDC2.5 mice resulted in equivalent disease kinetics (Fig. 4a) and severity (not shown). Transferring $CD4^+CD62L^+V\beta^+$ T cells from $Ocab^{-/-}$

bioRxiv preprint doi: https://doi.org/10.1101/2020.02.06.937839; this version posted March 14, 2020. The copyright holder for this preprint (which was not certified by peer review) is the author/funder. All rights reserved. No reuse allowed without permission.

and control NOD.BDC2.5 mice into NOD.Scid recipients also showed no difference between the experimental and control groups (Supplementary Fig. 4a). Negative results were also generated by transplanting total $CD4^+$ T cells into immunodeficient NCG recipients (Fig. 4b). We also tested the effect of T cell conditional OCA-B deletion in a different strain background, C57BL/6J, using the artificial membranous ovalbumin antigen expressed from the rat insulin promoter (RIP-mOVA)[36]. In this experiment, wild-type OVA-reactive $CD8^+$ OT-I T cells were transferred into either *Ocab*$^{fl/fl}$Cre^{CD4} or control *Ocab*$^{fl/fl}$ RIP-mOVA mice. Host $CD4^+$ T cells help transferred OT-I T cells promote T1D pathogenesis in this model[37]. Mice were then infected with Lm-OVA to induce strong and synchronous beta cell destruction and loss of glucose control (>400 mg/dL). No differences were observed (Supplementary Fig. 4b). These results indicate that OCA-B does not act analogously to transcription factors that act as a primary on/off switches, such as NF-AT. Knockouts of these factors would result in broad immunosuppression and protection from T1D in all models. Rather, our results suggest that the effects of OCA-B loss may protect from autoimmunity in specific contexts, including polyclonal contexts. To test this supposition, we also performed transplant experiments using total splenocytes from polyclonal NOD.*Ocab*$^{fl/fl}$Cre^{CD4} mice or controls. Using this transplant system, robust T1D protection with T cell-specific OCA-B loss was observed (Fig. 4c). This protection was associated with fewer IFNγ-expressing cytotoxic T cells in the islets of OCA-B T cell conditional NOD mice (Fig. 4d), and less insulitis in histological sections of pancreata (Fig. 4e,f).

NY8.3 transgenic mice express a CD8-restricted TCR directed towards $IGRP_{206\text{-}214}$ and manifest spontaneous T1D[38]. The NY8.3 clonotype was significantly attenuated in the islets of T cell conditional OCA-B deficient mice (Fig. 3c,d,e). We also crossed the *Ocab* germline allele NY8.3, passively monitoring *Ocab*$^{-/-}$ or littermate control *Ocab*$^{+/+}$ NY8.3 mice for T1D development. Significant protection was observed (HR=0.4472, p=0.0352), though the degree of protection was less than in polyclonal models (Fig. 4g). Together with the observed depletion of autoreactive CD8 clones from OCA-B deficient pancreatic islets, this result indicates that OCA-B promotes T1D in peripheral auto-reactive T cells in part directly through the $CD8^+$ cells. Using immunoblotting with OCA-B antibodies, we confirmed OCA-B expression in primary splenic C57BL/6 $CD8^+$ T cells. OCA-B is undetectable in naïve splenic $CD4^+$ cells but becomes induced with prolonged activation[4]. Unlike $CD4^+$ cells (Fig .4h, top panels), OCA-B^+ could be detected in naïve cells (Fig. 4h, lane 1). Expression was augmented more rapidly in $CD8^+$ cells upon T cell activation using CD3ε/CD28 antibodies (lane 2). Similar to $CD4^+$ cells, expression was stably maintained when the stimulus was removed and cells were rested with IL-2 (lane 6).

bioRxiv preprint doi: https://doi.org/10.1101/2020.02.06.937839; this version posted March 14, 2020. The copyright holder for this preprint (which was not certified by peer review) is the author/funder. All rights reserved. No reuse allowed without permission.

OCA-B deficiency promotes CD4$^+$ T cell anergy in vitro. Our scRNAseq data indicate that CD8-restricted TCR clones associated with T1D are depleted from the islets of OCA-B T cell conditional mice. In contrast, CD4-restricted clones were increased but associated with an anergic phenotype (Fig. 3e). Anergy is a peripheral tolerance mechanism in which T cells that encounter TCR signals without co-stimulation become nonfunctional to protect from autoreactivity[39, 40, 41]. Normal naïve primary CD4$^+$ T cells can be activated in culture by TCR and costimulatory receptor activation, e.g. with anti-CD3ε/CD28 antibodies. Providing TCR signals (via immobilized anti-CD3ε monoclonal antibodies) to naïve T cells in culture generates anergic responses[42]. Loss of Oct1, the transcription factor with which OCA-B docks, augments anergic responses in this assay[5]. Interestingly, OCA-B protein is induced to the same extent in naïve CD4$^+$ T cells stimulated with only anti-CD3ε antibodies as with co-stimulation (Fig.5a). To determine if OCA-B loss promotes anergic CD4$^+$ T cell responses, we stimulated naïve splenic CD4$^+$ T cells from germline knockout *Ocab*$^{-/-}$ and control *Ocab1*$^{+/+}$ animals ex vivo using plate-bound anti-CD3ε antibodies without co-stimulation, and restimulated the cells with PMA/ionomycin. Following restimulation, CD4$^+$ T cells lacking OCA-B generated 2.5-fold less IL-2 (Fig. 5b,c), indicating that OCA-B provides a barrier against anergic responses.

ICOS (Inducible T-cell Costimulator) has an important role in the induction of T cell anergy and is down-regulated by Oct1 loss in T cells[43, 44, 45]. Similarly in CD4$^+$ cells, elevated expression of FR4 and CD73 is associated with anergy and higher in Oct1-deficient compared to control cells[39, 46]. To determine whether OCA-B affects in the protein related to T cell anergy, we harvested pre-activated CD4$^+$CD44$^+$ T cells from the spleens of *Ocab*$^{fl/fl}$Cre^{CD4} and littermate control Cre^{CD4} animals, and re-stimulated them for 24 hr ex vivo using anti-CD3ε antibodies ± co-stimulation using anti-CD28 antibodies. CD4$^+$CD44$^+$FR4^{hi}CD73^{hi} anergic cells were ~2 fold more strongly induced in T cells lacking OCA-B (Fig. 5d). ICOS levels were similarly elevated in the OCA-B deficient condition (Fig. 5e). Additionally, and consistent with prior data[5], the expression of the activation marker CD25 was decreased (Fig. 5f). These results suggest that OCA-B loss creates a requirement for CD28 co-stimulation in secondary stimulation situations, effectively instituting higher immune checkpoint thresholds in order for cells to become fully re-activated.

Generation of an OCA-B peptide inhibitor. The normal T cell developmental and primary immune response phenotypes observed with OCA-B genetic deletion suggested the possibility of a "therapeutic window" in which targeting OCA-B pharmacologically would leave baseline immune function only

bioRxiv preprint doi: https://doi.org/10.1101/2020.02.06.937839; this version posted March 14, 2020. The copyright holder for this preprint (which was not certified by peer review) is the author/funder. All rights reserved. No reuse allowed without permission.

minimally affected. Drugs that target transcription factors and protein-protein interactions are now entering clinical use[47, 48]. Pre-clinical membrane-penetrating peptides have also been developed that successfully target transcription factors such as BCL6[49]. Based on the co-crystal structure of the Oct1 DNA-binding domain, the OCA-B N-terminus and consensus binding DNA[50], we applied rational-design principles to generate a membrane-permeable peptide inhibitor of OCA-B's downstream effector functions in order to target OCA-B pharmacologically.

In $CD4^+$ T cells, Oct1 interacts with Jmjd1a in a MEK/ERK-dependent manner[4, 6]. Oct1 contains two consensus ERK phospho-acceptor serines. The structure of the Oct1 DNA binding domain complexed with consensus octamer binding site DNA[51] reveals that these Oct1 serines are located in a flexible, solvent-exposed loop (the linker domain), which connects the two DNA binding sub-domains (Fig. 6a, red dashed line). In contrast with Oct1, OCA-B constitutively interacts with Jmjd1a[4]. The OCA-B N-terminus has been solved in complex with Oct1 and consensus octamer DNA[50]. The crystalized region of OCA-B is known to include regions critical for both Oct1 binding and transcription activity[52]. To identify potential Jmjd1a-interacting OCA-B regions, we aligned the full-length Oct1 and OCA-B amino acid sequences to a region of androgen receptor (AR) known to interact with Jmjd1a[53]. Human AR mutations that cause androgen insensitivity have been mapped to a cofactor interaction surface spanning residues 698-721[54]. Aligning this sequence to full-length Oct1 identified the linker domain as the top hit (Fig. 6b), implicating the Oct1 linker as a potential Jmjd1a-interacting surface. The alignment shows conservation of 3 out of 4 sites of deleterious AR mutation (asterisks) with Oct1. The mutation site that is not conserved is a consensus ERK target in Oct1, and a phospho-mimetic glutamic acid residue in AR (blue box). These findings suggest that the Oct1 linker domain constitutes a surface which, when phosphorylated by ERK, interacts with Jmjd1a.

As with Oct1, alignment with OCA-B identifies a potential Jmjd1a interacting surface (Fig. 6b). Unlike Oct1, an OCA-B glutamic acid residue (Glu30) aligns with AR, consistent with the finding that OCA-B constitutively interacts with Jmjd1a in the absence of ERK signaling[4]. Furthermore, the OCA-B residues aligning to AR lie on one side of a short, solvent-exposed alpha-helix (Fig. 6a). Glu30 (red), Leu31 (yellow), Arg34 (blue) and His38 (blue) may therefore constitute a Jmjd1a docking surface. These residues are conserved to humans (Fig. 6c). We mutated OCA-B L31 and R34 to alanines in a transient expression plasmid to test the effect on the Jmjd1a interaction, and transfected the double-point mutant or parent plasmid control into HCT116 cells, which do not express endogenous OCA-B. Control co-IP using Jmjd1a antibodies and wild-type OCA-B confirms the published interaction (Fig. 6d, lane 5), while the mutant OCA-B protein failed to interact (lane 8). The

bioRxiv preprint doi: https://doi.org/10.1101/2020.02.06.937839; this version posted March 14, 2020. The copyright holder for this preprint (which was not certified by peer review) is the author/funder. All rights reserved. No reuse allowed without permission.

mutant was expressed equivalently to WT in HCT116 cells (lanes 2, 3). These results show the importance of OCA-B residues 30-38 for the interaction with Jmjd1a.

To identify potential OCA-B competitive inhibitors, we synthesized three overlapping peptides corresponding to the OCA-B N-terminus (Fig. 6e, peptides #1, #2 (hereafter called "JumOCA") and #3), as C-terminal fusions to the HIV Tat protein for membrane permeability[55]. Initial preparations were conjugated to FITC to track the peptide. Incubating peptides with total splenic or pancreatic $CD3^+$ T cells in culture with 45 μM Tat-fused peptide for 15 min resulted in significant concentration. Control OVA-fused peptide showed no such effect (Supplementary Fig. 5). We then treated splenic $CD4^+$ T cells with the Tat-fused peptides (lacking FITC) in ex vivo culture. Prior work has shown that 6 hr restimulation of resting but previously activated cells reveals sensitivity to OCA-B loss[4]. Using this assay with 50 μM JumOCA peptide (every other day with media changes during rest and restimulation) inhibited *Il2* mRNA expression relative to β-actin by ~10-fold (Fig. 6f, compare Tat peptide to JumOCA). Although treated cells showed no obvious changes in viability, morphology or expansion during the course of the assay (not shown), there was a 2-3-fold nonspecific diminution of activity associated with unfused Tat peptide (Fig. 6f, compare Tat peptide with no peptide). The Tat membrane-penetrating peptide has been associated with toxicities[49, 56, 57]. Similar results were obtained with the larger peptide #3 but not with peptide #1 (not shown). Peptide #1 is missing residues important for the Jmjd1a interaction based on mutagenesis (Fig. 6b). For all further experiments, we exclusively used the JumOCA peptide.

We then synthesized a Tat-conjugated peptide using a scrambled JumOCA sequence. This peptide has the same amino acid composition, mass and pI, but lacks the OCA-B primary amino acid sequence and should not be able to efficiently compete for Jmjd1a. We used the Tat-only, scrambled and JumOCA peptides in assays similar to Fig. 6f, except using flow cytometry to assay endpoint IL-2 production. JumOCA significantly inhibited IL-2 production relative to the scrambled control, however there were significant toxicities associated with both the scrambled and Tat-only peptides relative to vehicle (Fig. 6g). An example mouse from this experiment is shown in Fig. 6h.

The above results are consistent with the JumOCA peptide operating through a Jmjd1a competitive inhibition mechanism. To test this directly, we used scrambled, double point mutant and wild-type (JumOCA) peptides lacking Tat in a Jmjd1a co-IP assay. We subjected lysates from mouse M12 B cells, which expresses endogenous OCA-B, to immunoprecipitation with Jmjd1a antibodies, resulting in efficient OCA-B co-IP (Fig. 6i, lane 3). Incubation of precipitated material with scrambled

bioRxiv preprint doi: https://doi.org/10.1101/2020.02.06.937839; this version posted March 14, 2020. The copyright holder for this preprint (which was not certified by peer review) is the author/funder. All rights reserved. No reuse allowed without permission.

or double point mutant peptides had no effect on OCA-B co-immunoprecipitation (lanes 4-5), while the same concentration of JumOCA peptide efficiently blocked OCA-B recovery (lane 6).

An OCA-B peptide inhibitor protects NOD mice from newly-arisen diabetes. By the time symptoms arise in NOD mice, 90-95% of beta cells have been destroyed. Remaining beta cells are rendered nonfunctional due to insulitis. Alleviating this inflammation provides a "honeymoon period" during which glucose homeostasis can be restored. We treated 14-18 week-old littermate female NOD mice whose glucose levels were newly-risen above 225 mg/dL but still below 275 mg/dL with three intravenous injections of 10 mg/kg peptide or Tat-only peptide control. Injections were spaced 12 hr apart. 12 hr after the final injection, blood glucose was collected and flow cytometry performed on the pancreas and PLNs. Strikingly, the inhibitor reversed elevated blood glucose (Fig. 7a). Control peptide at the same concentration had no effect. Islet T cell infiltration and pro-inflammatory IFNγ and IL-17A cytokine production were strongly reduced by JumOCA peptide treatment compared to controls (Fig. 7b,c). In contrast to the pancreas, PLNs showed no change in T cell numbers or percentages (Fig. 7d) but similar changes in pro-inflammatory cytokine production (not shown). These data provide evidence that targeting OCA-B is a valid strategy to treat emerging T1D, potentially with minimal side effects, and identify a first-generation inhibitor that is efficacious in vivo.

bioRxiv preprint doi: https://doi.org/10.1101/2020.02.06.937839; this version posted March 14, 2020. The copyright holder for this preprint (which was not certified by peer review) is the author/funder. All rights reserved. No reuse allowed without permission.

Discussion

Here we show that targeting OCA-B genetically or pharmacologically can block T1D in mouse models. OCA-B is a transcriptional coregulatory protein named for its strong expression in the B cell lineage, where it is dispensable until after B cell activation, where it is essential for the generation of germinal centers[58]. OCA-B is not expressed during thymic development or in naïve CD4 T^+ cells, but is stably induced upon T^+ cell activation. In contrast, OCA-B is expressed in $CD8^+$ T cells, albeit at lower levels compared to activated T cells. In both populations, OCA-B expression is maintained after T cell stimulation has ceased.

In $CD4^+$ T cells, OCA-B associates with the POU-domain transcription factor Oct1 at ~150 immunomodulatory genes – among them *Il2*, *Ifng*, *Il17a* and *Csf2* (*Gmcsf*). Unlike transcription factors such as NF-AT, AP-1 and NF-kB that act as primary "on" switches via direct gene activation, OCA-B removes inhibitory chromatin modifications to establish permissive chromatin environments that allow for silent but previously activated targets to be robustly expressed later[4, 6]. More specifically, OCA-B interacts with Jmjd1a/Kdm3a, a histone lysine demethylase that removes inhibitory histone H3 lysine 9 methyl marks. OCA-B target gene expression is unchanged upon primary stimulation of cultured Oct1- or OCA-B-deficient T cells, but upon secondary stimulation (a model of antigen reencounter) the normally observed increased expression does not occur[4, 6]. In vivo, OCA-B loss leaves T cell development and pathogen response unaffected, but impairs the establishment of new central memory $CD4^+$ T cells. The few cells that are formed respond poorly to antigen re-encounter[4]. Repeated antigen encounters that drive high levels of proinflammatory cytokines are a key feature of autoimmunity. In both mice and humans, memory or memory-like cells can underlie autoimmunity including T1D[59, 60, 61].

The NOD model of T1D is spontaneous but only partially penetrant, much like the human disease[62]. 60-80% of female NOD mice develop T1D in standard environments[22]. We find that prediabetic OCA-B T cell deficient NOD mice harbor normal T cell numbers and similar TCR specificities in their PLNs, consistent with prior observations that OCA-B deficient T cells are immunocompetent[4]. Nevertheless, T cell conditional OCA-B knockouts are fully protected from spontaneous T1D. Protection is associated with reduced islet leukocyte infiltration and reduced proinflammatory cytokine expression. Whole-body NOD *Ocab* knockouts are also protected from T1D, though to a lesser degree. Prior work showed that OCA-B whole-body knockout protects mice in a MOG/EAE model of multiple sclerosis[63]. In contrast, a second study showed that OCA-B whole body knockout exacerbates systemic, antibody-driven autoimmunity in *Sanroque* mice[64]. The protective vs. exacerbating effects in these models may be due to effects on BCR repertoire[65]. T cell-

bioRxiv preprint doi: https://doi.org/10.1101/2020.02.06.937839; this version posted March 14, 2020. The copyright holder for this preprint (which was not certified by peer review) is the author/funder. All rights reserved. No reuse allowed without permission.

specific knockout of Oct1, a transcription factor with which OCA-B docks, blocks EAE but leaves responses to infection with neurotropic viruses intact[5]. Together these data indicate that in T cells Oct1 and OCA-B promote autoimmunity including T1D, but that their role in B cells may be more complex. OCA-B is typically expressed ~50-fold higher in B cells compared to T cells. A correctly calibrated dose of competitive inhibitor could therefore be used to selectively blunt T cell-mediated autoimmunity.

scRNAseq experiments reveal decreased neutrophil infiltration and an increase in the percentage of T cells with a naïve phenotype in prediabetic OCA-B conditional knockout islets. Gene expression changes were also identified that were consistent with antidiabetogenic effects of OCA-B T cell knockout. For example, the remaining islet neutrophils in knockout mice show strong reductions in *Cxcl2* expression compared to littermate controls. Cxcl2 is a potent neutrophil chemoattractant that promotes T1D in vivo[66, 67], and therefore reductions in Cxcl2 may contribute to the reduced neutrophil representation. Strikingly, OCA-B T cell deficient mice also lacked T1D-associated TCR clones in their activated/memory CD8 pool. CD4 clonotypes associated with T1D were present, but associated with anergy. Consistently, OCA-B loss promotes $CD4^+$ T cell anergy in vitro.

BDC2.5 and NY8.3 TCR transgenic mice are simplified monoclonal systems that allow easy tracking of uniform T cell responses to antigens in vivo[68]. To test if OCA-B loss confers protection in simplified monoclonal systems, we crossed the germline OCA-B null allele to these models, as well as to RIP-mOVA transgenic mice on the C57BL/6 background. The latter mice express synthetic membranous chicken ovalbumin in their thymi and pancreatic beta cells[69]. We crossed whole-body null mice to the BDC2.5 transgenic line[70], which expresses a CD4-restricted TCR specific for a hybrid insulin-chromogranin A peptide[71]. BDC2.5 autoreactive cells migrate to the islets and cause insulitis beginning at 3-4 weeks. Due in part to Tregs that have escaped allelic exclusion, in many animals insulitis is limited and does not progress to full-blown T1D. However, transferring $CD4^+CD62L^+V\beta^+$ or $CD4^+CD25^-$ T cells from BDC2.5 donor mice into NOD.SCID recipients results in rapid (7-10 d) disease onset[34]. Transplants from both control and OCA-B null NOD/BDC2.5 mice resulted in disease with similar kinetics. Identical results were also generated by depleting $CD25^+$ Tregs, or by transplanting total $CD4^+$ T cells into immunodeficient NCG recipient mice. OCA-B loss also had no effect using the RIP-mOVA model on the C57BL/6 background. This model expresses a synthetic antigen, membranous chicken ovalbumin, in thymic epithelial and pancreatic beta cells[36].

In contrast to BDC2.5 and RIP-mOVA, NY8.3 transgenic mice carry a monoclonal CD8-restricted TCR directed towards $IGRP_{206-214}$ and manifest spontaneous T1D[38]. Unlike BDC2.5

bioRxiv preprint doi: https://doi.org/10.1101/2020.02.06.937839; this version posted March 14, 2020. The copyright holder for this preprint (which was not certified by peer review) is the author/funder. All rights reserved. No reuse allowed without permission.

transplant models, OCA-B T cell conditional NY8.3 mice showed significant protection, though unlike polyclonal NOD mice protection was incomplete. Cumulatively, the results are consistent with a model in which OCA-B loss does not simply block T cell functionality, but rather desensitizes autoreactive T cells. Because transgenic TCR models have fixed affinities to antigens that can be present throughout disease or arise at specific points during disease etiology, they result in graded levels of disease. By shifting the autoreactivity of different T cells along a spectrum of disease potentials, OCA-B loss can result in full or partial protection in models with low and intermediate disease thresholds, whereas models with high disease potentials remain autoreactive. Although protection in some of the more severe models is likely to be inseparable from immunodeficiency, our results show that genetic ablation of OCA-B strongly protects NOD animals from spontaneous T1D, and results in graded protection that drops off with severity of the model. These properties make OCA-B a promising target for pharmaceutical inhibition.

Recent work indicates that the prevailing idea that transcription regulators and protein-protein interactions are "undruggable" is erroneous[47, 48, 72]. Pre-clinical membrane-penetrating peptides have also been developed that successfully target transcription factors such as BCL6[49]. We applied rational-design principles to generate a membrane-permeable competitive peptide inhibitor of the interaction between OCA-B and a downstream effector, Jmjd1a/Kdm3a. This inhibitor corresponds to a region of the OCA-B N-terminus, which is known to include residues critical for Oct1 binding and transcription activity[52]. We tested the effect of this inhibitor, termed JumOCA, on T1D onset and severity. The JumOCA sequence does not coincide with other sequences in the human or mouse proteome and is not predicted to be strongly immunogenic. Peptide administration into NOD mice protected animals from newly-arisen T1D and significantly reduced islet-infiltrating T cell numbers and cytokine production, while having more mild effects on the PLNs. OCA-B levels in B cells are at least 50-fold higher than in T cells (immgen.org)[73], making it likely that the observed effects are due to inhibition in T cells. The preservation of normal PLN functionality both with peptide treatment and OCA-B genetic ablation suggests a potential therapeutic window in which targeting OCA-B may leave baseline immune function unaffected. While these peptides are unlikely to be used in a clinical setting, they offer proof-of-principle for OCA-B as a therapeutic target, and can be used as tools for the further development of therapeutics.

bioRxiv preprint doi: https://doi.org/10.1101/2020.02.06.937839; this version posted March 14, 2020. The copyright holder for this preprint (which was not certified by peer review) is the author/funder. All rights reserved. No reuse allowed without permission.

Methods

Laboratory mice. NOD/ShiLtJ, NOD.Scid (NOD.Emv302/2.CB17-Prkdcscid), BDC-2.5 TCR transgenic, NY8.3 TCR transgenic and all breeder mice were maintained in a specific pathogen-free research colony. NCG (NOD-Prkdc^{em26Cd52}Il2rg^{em26Cd22}/NjuCrl) mice were purchased from Charles River Laboratories. NOD.Cre^{CD4} breeding pairs were a gift from Alexander Chervonsky (University of Chicago). All animal experiments were approved by the University of Utah Institutional Animal Care and Use Committee (IACUC approval 17-05008).

Generation of *Ocab* (*Pou2af1*) conditional mice. *Pou2af1*$^{tm1a(KOMP)Wtsi}$ mice were provided by the knockout mouse project (KOMP) repository (University of California, Davis). Mice were derived from embryonic stem cell clone EPD0761_3_B03, generated by the Wellcome Trust Sanger Institute. These cells were derived from C57BL/6N mice, but subsequent mouse crosses were to C57BL/6J (>20 generations) for the RIP-mOVA model and NOD (four congenic backcrosses plus an additional backcross to NOD.Cre^{CD4}). The embryonic stem cells contain a CSD-targeted allele[74]. The presence of WT (582 bp) and Post-FLP (700 bp) alleles was determined by PCR using CSD-Pou2af1-F and CSD-Pou2af1-ttR primers. The presence of the null (801 bp) allele was determined using CSD-Pou2af1-F and CSD-Pou2af1-R primers. The presence of the floxed (359 bp) allele was determined using CSD-Lox-F and CSD-Pou2af1-R primers. Primer sequences were as follows: CSD-Pou2af1-F, 5'TACAGAGAGACTAGACACGGTCTGC; CSD-Pou2af1-R, 5'GATGAGGACTCTGGGTTCAGAGAGG; CSD-loxF, 5'GAGATGGCGCAACGCAATTAATG; CSD-Pou2af1-ttR, 5'AGAAGGCCTCGTTACACTCCTATGC. *Ocab* conditional mice were bred with mice expressing Cre under the control of the CD4 promoter.

Backcrossing *Ocab* germline null and conditional mice to the NOD background. To generate *Ocab*$^{-/-}$ and *Ocab* conditional mice on the NOD background, the previously described C57BL/6 *Ocab* germline null allele[20] and the newly-generated *Ocab* conditional allele were backcrossed to NOD ShiLt/J mice using congenic markers based on Mouse Genome Informatics (http://www.informatics.jax.org) (Supplementary Table 1).

Diabetes development and assessment. Diabetes was monitored using blood glucose test strips (Contour, Bayer). Mice with blood glucose levels >250 mg/dL were considered diabetic.

bioRxiv preprint doi: https://doi.org/10.1101/2020.02.06.937839; this version posted March 14, 2020. The copyright holder for this preprint (which was not certified by peer review) is the author/funder. All rights reserved. No reuse allowed without permission.

Leukocyte isolation and intracellular cytokine staining. Pancreatic lymph nodes were grinded and passed through a nylon strainer. Pancreatic leukocytes were isolated as described previously[75]. Briefly, pancreata were chopped and digested using collagenase IV (1 mg/mL, Gibco) in DMEM containing 1% fetal bovine serum (FBS, Rocky Mountain Biologicals) and 10 units of DNase I for 15 min at 37°C. The digested tissues were passed through a 70 μm strainer. Red blood cells were lysed by ACK (Ammonium-Chloride-Potassium) lysis buffer (150 mM NH_4Cl, 10 mM $KHCO_3$, 0.1 mM Na_2EDTA). For intracellular cytokine staining, cell suspensions in RPMI medium supplemented with 10% FBS were re-stimulated for 4 hr with phorbol 12-myristate 13-acetate (PMA, Sigma, 50 ng/mL) and ionomycin (Sigma, 1 μg/mL) in the presence of Brefeldin-A (GolgiPlug, BD Bioscience, 1 μl/ml), and fixed by cell fixation/permeabilization solution (BD Cytofix/Cytoperm) according to the manufacturer's protocol. Antibodies used for flow cytometry were as follows: FITC-conjugated anti-mouse CD4, PE-conjugated anti-mouse CD45, PE-conjugated anti-mouse FR4 (Biolegend), PerCP-conjugated anti-mouse CD8a, APC-conjugated anti-mouse IFNγ, PE-conjugated anti-mouse IL-17, PerCP-conjugated anti-mouse CD11b, APC-conjugated anti-mouse F4/80, PE-conjugated anti-mouse Gr-1, PE-conjugated anti-mouse ICOS (eBioscience), PerCP-conjugated anti-mouse FoxP3, V450-conjugated anti-mouse CD73 (BD Bioscience) FITC-conjugated anti-mouse Vβ8.1/8.2 (Invitrogen).

T cell adoptive transfer. 6–8 wk old NOD.Scid recipient mice were injected retro-orbitally with 2×10^5 of splenic $CD4^+CD25^-$ T cells from pre-diabetic *Ocab*$^{-/-}$ or *Ocab*$^{+/+}$ NOD.BDC2.5 donors (6–8 wk old, sex-matched). T cells were purified using a $CD4^+CD25^+$ T cell isolation kit (Miltenyi). For $CD4^+CD25^+Foxp3^+$ T cells, 1.5×10^6 purified splenic $CD4^+$ T cells from pre-diabetic, BDC2.5 transgenic NOD.*Ocab*$^{-/-}$ or NOD.*Ocab*$^{+/+}$ mice were transferred to sex-matched 6-8 wk old NCG recipients (University of Utah pre-Clinical Resource Core) as previously described[35]. For total splenic transfer experiments, 5×10^6 splenocytes from pre-diabetic NOD.*Ocab*$^{fl/fl}$ or NOD.*Ocab*$^{fl/fl}$Cre^{CD4} mice were transferred into sex-matched 6-8 week-old NOD.Scid recipients mice as described previously[35].

In vivo Treg depletion. Anti-CD25 antibody in PBS (1 mg/mouse, Clone PC61, BioXCell) was administered intraperitoneally to NOD.*Ocab*$^{fl/fl}$ or NOD.*Ocab*$^{fl/fl}$Cre^{CD4} mice twice (10 and 17 d after birth) as previously described[32].

In vitro culture of CD4 T cells. For anergic cell induction, spleens were harvested from NOD.*Ocab*$^{fl/fl}$Cre^{CD4} or control NOD.*Ocab*$^{fl/fl}$ animals. Single-cell suspensions were generated by

bioRxiv preprint doi: https://doi.org/10.1101/2020.02.06.937839; this version posted March 14, 2020. The copyright holder for this preprint (which was not certified by peer review) is the author/funder. All rights reserved. No reuse allowed without permission.

559 grinding and passage through 70 μm strainers. $CD4^+$ T cells were isolated using a mouse $CD4^+$ T cell
560 isolation kit (Miltenyi Biotec). Isolated $CD4^+$ T cells were cultured and stimulated with 5 μg/ml plate-
561 bound anti-CD3ε (BD Bioscience) and/or 2 μg/ml anti-CD28 antibodies (eBioscience) as described
562 previously[5]. For OCA-B inhibitor peptide treatments, naïve CD4 T cells were isolated from WT
563 C57BL/6 mice using a mouse naïve $CD4^+$ T cell isolation kit (Miltenyi Biotec) and cultured as
564 described previously[6]. For the in vitro experiments with OCA-B inhibitor peptides, indicated
565 concentrations of OCA-B inhibitor or control peptides were incubated with cells, with media changes
566 every 2 days after primary stimulation. Activation of C57BL/6 $CD4^+$ cells and subsequent profiling of
567 anergic responses was performed identically to[5].
568
569 **Single cell RNA sequencing.** $CD3^+$ T cells were isolated from 8 week-old NOD.*Ocab*$^{fl/fl}$ or
570 NOD.*Ocab*$^{fl/fl}$Cre^{CD4} females using a pan T cell isolation kit (Miltenyi). $CD45^+$ pancreatic leukocytes
571 were isolated from 12 week-old NOD.*Ocab*$^{fl/fl}$ or NOD.*Ocab*$^{fl/fl}$Cre^{CD4} females were isolated by flow
572 cytometry using a FACS Aria instrument (Becton-Dickinson). For each condition, cells were isolated
573 from three mice and combined. Cells were processed using the 10× Genomics Chromium platform
574 according the manufacturer's instructions. Paired-end high-throughput sequencing (125 cycles) was
575 performed via an Illumina NovaSeq instrument. Sequencing reads were processed by using 10×
576 Genomics CellRanger pipeline and further analyzed using the Seurat R package. Analysis of cells used
577 a standard filtering protocol removing cells with unique feature counts of >4,000 or <500, as well as
578 cells that have >5% mitochondrial counts (indicative of dead cells). No more than 15% of total cells
579 were removed by this process.
580
581 **OCA-B mutagenesis and co-IP.** For generation of the OCA-B double point mutant, a plasmid
582 transiently expressing human OCA-B, pCATCH-Bob.1[76], was sequentially mutagenized using
583 QuickChange (ThermoFisher). Correct mutagenesis and lack of additional mutations was confirmed by
584 resequencing. Protein expression was confirmed by transiently transfect HCT116 cells, which do not
585 express endogenous OCA-B. HCT116 lysate preparation, co-immunoprecipitation of OCA-B and
586 endogenous Jmjd1a, and immunoblot detection was performed using the same conditions as
587 described[4]. For co-IP using M12 cells, lysis buffer consisted of 50 mM Tris-Cl, pH 7.4, 150mM NaCl,
588 0.5%NP-40, 1 mM EDTA,1 mM EGTA, plus protease/phosphatase inhibitors (PhosSTOP, Roche).
589 Lysates were incubated with 2.5 μg Jmjd1A antibody (Bethyl) and protein-G Dynabeads
590 (ThermoFisher) in lysis buffer containing 20% glycerol overnight at 4°C. After overnight incubation,

bioRxiv preprint doi: https://doi.org/10.1101/2020.02.06.937839; this version posted March 14, 2020. The copyright holder for this preprint (which was not certified by peer review) is the author/funder. All rights reserved. No reuse allowed without permission.

591 the indicated concentrations of peptide or PBS vehicle was added and incubated for a further 3 hr at
592 4°C prior to bead precipitation and washing 3× in lysis buffer plus 20% glycerol. Co-precipitated
593 OCA-B was analyzed by SDS-PAGE and immunoblot.
594
595 **OCA-B inhibitor peptide synthesis.** Unique chemically synthesized peptide sequences were as
596 follows: Peptide#1, ARPYQGVRVKEPVK; Peptide#2/JumOCA, VKELLRRKRGH; Peptide#3,
597 ARPYQGVRVKEPVKELLRRKRGH; Scrambled peptide, VLREKGKRHLR. Peptides were
598 synthesized with and without a covalent C-terminal linker and Tat membrane-penetrating peptide
599 (GSG-GRKKRRQRRRGY). Fmoc protected amino acids were obtained from Protein Technologies
600 Inc. 1-[Bis(dimethylamino)methylene]-1H-1,2,3-triazolo[4,5-b]pyridinium 3-oxid
601 hexafluorophosphate (HATU) was purchased from Chemimpex Inc. H-Rink-Amide-ChemMatrix
602 (RAM) was purchased from Biotage. N,N-diisopropylethylamine (DIEA), dichloromethane (DCM),
603 triisopropylsilane (TIS) were purchased from Sigma Aldrich. Dimethylformamide (DMF),
604 trifluoroacetic acid (TFA), acetonitrile (ACN), and ethyl ether were purchased from Fisher Scientific.
605 Peptides were synthesized using automated Fmoc SPPS chemistry on synthesizer (Syro I). Briefly, 220
606 mg of RAM resin (Loading = 0.45 mmol/g) was swelled in DCM for 15 min and followed by adding in
607 a solution of specific Fmoc protected amino acid (AA = 0.1 mmol, DIEA = 0.2 mmol in DCM = 4 mL)
608 and incubated at room temperature for 1.5 h. Then the resin was washed with DMF and DCM and
609 incubated with 5 mL of DCM containing 16% v/v MeOH and 8% v/v DIEA for 5 min. This action was
610 repeated for 5 times before thoroughly washed with DCM and DMF. Then the resin was set to
611 synthesizer for automated synthesis. Coupling reactions were performed using HATU (5 eq.), DIPEA
612 (10 eq.) and amino acid (5 eq.) in DMF with 15 min heating to 70 oC (50 oC for Cys). Deprotection
613 reaction was performed using 20% (v/v) Piperidine in DMF, 5 min rt for 2 rounds. Peptides were
614 cleaved from the resin by treatment with a cocktail buffer (3 mL/0.1 mmol, TFA:H2O:TIS:EDT =
615 95:2:2:1) for 2.5 h. Peptide-TFA solution was then filtered and precipitated in cold ether, and
616 centrifuged and washed with ether twice and vacuum-dried. The crude product was then purified by
617 RP HPLC. Peptides characterization was performed by LC/MS on an Xbridge C18 5 μm (50 x 2.1
618 mm) column at 0.4 mL/min with a water/acetonitrile gradient in 0.1% formic acid on an Agilent 6120
619 Quadrupole LC/MS system. Fractions collected from HPLC runs were also analyzed by LC/MS. The
620 purified fractions containing the targeted product were collected and lyophilized using a Labconco
621 Freeze Dryer. All samples were analyzed by the following conditions: Preparative reverse phase HPLC
622 of crude peptides was performed on a Jupiter 5 μ C18 300 Å (250×10 mm) column at 3 mL/min with a
623 water/acetonitrile (ACN) gradient in 0.1% TFA on an Agilent 1260 HPLC system. Purity, isomer co-

bioRxiv preprint doi: https://doi.org/10.1101/2020.02.06.937839; this version posted March 14, 2020. The copyright holder for this preprint (which was not certified by peer review) is the author/funder. All rights reserved. No reuse allowed without permission.

injection and stability checks were performed on HPLC on Phenomenex Gemini C18 3 µm (110 Å 150×3 mm) column.

OCA-B inhibitor peptide treatment. Anesthetized pre-diabetic WT NOD females with glucose levels newly-risen to between 225 to 275 mg/dL were treated with the inhibitor or control peptides by intravenous (retro-orbital) injection, 3 times every 12 hr. Blood glucose levels were measured at every injection. 4 hr after the last injection, pancreata and pancreatic lymph nodes (PLNs) were collected and cell populations were analyzed by flow cytometry.

Histology. Formalin-fixed pancreatic tissues were embedded in paraffin. H&E-stained sections were scored for islet inflammation based on published precedents[77]: 0, sparse surrounding sentinel leukocytes, no insulitis; 1, peri-islet leukocytes; 2, some into islet, <50% of islet area; 3, islet insulitis with >50% of islet area occupied by leukocytes; 4, islets destroyed with fibrotic remnants.

Statistical analyses. All error bars denote ±SEM. Two-tailed student T-tests were used to ascribe statistical significance. For all figures, *=*p*-value ≤0.05; **=*p*-value ≤0.005.

bioRxiv preprint doi: https://doi.org/10.1101/2020.02.06.937839; this version posted March 14, 2020. The copyright holder for this preprint (which was not certified by peer review) is the author/funder. All rights reserved. No reuse allowed without permission.

Acknowledgements

We thank P. Santamaria, M. Williams, M. Bettini and F. Gounari for critical reading of the manuscript. We thank A. Chervonsky (U. Chicago) for the gift of NOD.Cre^{CD4} mice. We thank J. Marvin and the University of Utah Health Sciences Center Flow Cytometry Core facility for assistance with flow cytometry. We thank M. Hanson and the University of Utah Health Sciences DNA/peptide synthesis core. This work was supported by grants to DT from the Praespero Foundation, Juvenille Diabetes Research Foundation (1-INO-2018-647-A-N) and National Institutes of Health (R01-AI100873).

Author's contributions

DT conceived the study and designed experiments, supervised the study, and provided administrative, technical and material support. HK, AS, AI and JLJ acquired and interpreted the data. JP performed high-level analysis of scRNAseq and TCR clonotype data. CG helped generate critical reagents. BDE, DH-CC, XH and PJ provided material and intellectual support. All authors were involved in writing, reviewing and revising the manuscript.

bioRxiv preprint doi: https://doi.org/10.1101/2020.02.06.937839; this version posted March 14, 2020. The copyright holder for this preprint (which was not certified by peer review) is the author/funder. All rights reserved. No reuse allowed without permission.

Figure legends

Fig. 1 | Loss of OCA-B protects NOD mice from T1D. a, Targeting event. Crossing with FLP^{Rosa26} results in conditional (*fl*) allele. Primer-pairs used for genotyping are depicted with arrows. **b**, Example genotyping of the targeted allele and recombination events. Founder animal is in lane 2. The primer-pairs shown in (a) were used. **c**, The *Ocab* (*Pou2af1*) conditional allele was crossed to Cre^{CD4}. Total splenic $CD4^+$ T cells were isolated from an $Ocab^{fl/fl}Cre^{CD4}$ animal or a $Ocab^{+/fl}Cre^{CD4}$ littermate control, and stimulated for 2 d in vitro using plate-bound CD3ε and soluble CD28 antibodies. An OCA-B immunoblot of stimulated total T cells is shown. β-actin is shown as a loading control. **d**, Kaplan-Meier plot of diabetes-free survival in littermate female NOD.$Ocab1^{fl/fl}Cre^{CD4}$ (n=12) and NOD.$Ocab1^{fl/fl}$ (n=14) mice. Diabetes criterion was ≥250 mg/dL blood glucose. HR=hazard ratio. **e**, Avearage blood glucose levels from mice shown in panel (c) is shown. **f**, Percent diabetes-free survival in germline knockout NOD.$Ocab^{-/-}$ (n=16) and control NOD.$Ocab^{+/+}$ (n=17) mice were plotted based blood glucose cutoff of ≥250 mg/dL.

Fig. 2 | NOD.*Ocab* conditional mice have fewer islet IFNγ expressing CD8 T cells and macrophages, and more Tregs compared to controls. a, Pancreatic islet leukocytes were isolated from 8 week- or 24 week-old littermate female NOD.$Ocab1^{fl/fl}Cre^{CD4}$ (8 week; n=3, 24 week; n=5) or NOD.$Ocab1^{fl/fl}$ (8 week; n=3, 24 week; n=4) mice and analyzed by flow cytometry. Mean $CD45^+CD11b^+F4/80^+$ cell frequencies are depicted. **b**, Frequencies of $CD45^+CD11b^+F4/80^+$ cells from representative animals in panel (a) are shown. Plots were gated on $CD45^+$ cells. **c**, Mean percentages of total pancreatic-infiltrating $CD8^+$ T cell in 12 week-old NOD.$Ocab1^{fl/fl}Cre^{CD4}$ or control NOD.$Ocab1^{fl/fl}$ mice are plotted. Cells were independently purified from 3 pancreata and gated on $CD45^+$. **d**, IFNγ expressing $CD8^+$ T cell percentages in 16 week old-NOD.$Ocab1^{fl/fl}Cre^{CD4}$ (n=3) and littermate control islets (n=5) are shown. **e**, Percentages of FoxP3-expressing $CD4^+$ T cells in pre-diabetic (8 week) NOD.*Ocab* conditional and control female mice are plotted. N=3 for each group. Mean of results is shown. **f**, NOD.$Ocab^{fl/fl}$ or NOD.$Ocab^{fl/fl}Cre^{CD4}$ pups were treated with anti-CD25 antibodies intraperitoneally on day 10 and 17 after birth to deplete Tregs (red arrows). Mice were monitored for T1D emergence as in Fig. 1.

Fig. 3 | T cell conditional OCA-B loss reduces the numbers of activated, autoreactive pancreatic islet T cells. a, scRNAseq was performed using total islet $CD45^+$ cells from prediabetic

bioRxiv preprint doi: https://doi.org/10.1101/2020.02.06.937839; this version posted March 14, 2020. The copyright holder for this preprint (which was not certified by peer review) is the author/funder. All rights reserved. No reuse allowed without permission.

686 NOD.*Ocab*$^{fl/fl}$Cre^{CD4} or control NOD.*Ocab*$^{fl/fl}$ mice (n=3 for each group). Cell populations were plotted
687 using UMAP (Seurat R package) and percentages in each cluster are shown for each genotype.
688 Different populations were identified using Seurat R package function FindMarkers. **b**, Four
689 populations from panel (a) were analyzed for differential gene expression. Identified genes are shown
690 as a scatter plot. Significantly differentially expressed genes (adjusted *p*-value <0.05) are shown in red.
691 **c**, UMAP plots similar to (a) are shown, except cells expressing TCR clonotype 13-3 are shown. The
692 non-naïve (activated+memory) CD8$^+$ cell population identified in (a) is shown in red. **d**, Percent
693 contribution of the top 21 identified TCR clonotypes to total activated+memory CD8$^+$ cells is shown.
694 The V genes comprising the top 6 clonotypes are also shown. **e**, Cells positive for clonotypes 1-5 are
695 shown for two clusters, non-naïve (activated+memory) CD8$^+$ T cells and CTLA4$^+$FR4$^+$ anergic cells
696 (consisting of mostly CD4$^+$ cells). For each cluster, positive cells are shown in dark blue. An overlay
697 of control and OCA-B deficient cell populations is shown, however because each clonotype is only
698 observed in a single genotype (panel d), all cells can be mapped back entirely to OCA-B deficient or
699 control (clonotypes 1 and 4: OCA-B deficient; clonotypes 2, 3 and 5: control).
700
701 **Fig. 4 | OCA-B loss protects NOD mice from T1D in spontaneous and polyclonal splenocyte**
702 **transfer models but not in monoclonal transfer models. a**, 2×10^5 purified CD4$^+$CD25$^-$ splenic T
703 cells from NOD.BDC2.5.*Ocab*$^{-/-}$ or control NOD.BDC2.5.*Ocab*$^{+/+}$ donors were injected retro-orbitally
704 into NOD.Scid (n=6 for each group) mice. Diabetes-free survival (≥250 mg/dL) is shown. **b**, 1.5×10^6
705 purified splenic total CD4$^+$ T cells from NOD.BDC2.5.*Ocab*$^{-/-}$ or control donors were transferred into
706 NCG mice (n=5 for each group). Mice were monitored for diabetes development. **c**, Total NOD
707 splenocytes (5×10^6) from prediabetic 6- to 8-wk-old sex-matched NOD.*Ocab1*$^{fl/fl}$Cre^{CD4} or control
708 NOD.*Ocab1*$^{fl/fl}$ donors were adoptively transferred into sex-matched NOD.Scid (n=7 for each group)
709 recipients. Diabetes incidence rates are shown. **d**, At 13 weeks post-transfer, the proportion of IFNγ-
710 expressing CD8$^+$ T cells was assessed by flow cytometry in pancreata isolated from mice receiving
711 splenocytes from NOD.*Ocab1*$^{fl/fl}$Cre^{CD4} or NOD.*Ocab1*$^{fl/fl}$ donors in panel (c). **e**, Pancreata from the
712 same mice as in (d) were fixed, sectioned and H&E stained. Pathological scores are shown based on 6-
713 7 islets per slide, 3 slides per mouse and 3 mice in each group (>60 islets per group). **f**, Example
714 pancreatic images from endpoint animals. Yellow arrows indicate islet positions. Images were
715 collected at 10× magnification. **g**, The *Ocab* null allele was crossed to NY8.3 TCR transgenic mice.
716 Spontaneous T1D was measured in female *Ocab*$^{-/-}$ (n=20) or control *Ocab*$^{+/+}$ (n=12) littermates. **h**,
717 Naïve CD4$^+$ or CD8$^+$ T cells were isolated from C57BL/6 spleens and stimulated for up to two days in

bioRxiv preprint doi: https://doi.org/10.1101/2020.02.06.937839; this version posted March 14, 2020. The copyright holder for this preprint (which was not certified by peer review) is the author/funder. All rights reserved. No reuse allowed without permission.

vitro using anti-CD3ε and CD28 antibodies. Cells were then washed and replated in the presence of exogenous IL-2. After 8 days rest in culture, cells were restimulated for 6 hr. Lysates were prepared from each step and subjected to OCA-B immunoblotting to assess changes in expression. Oct1 and β-actin are shown as controls.

Fig. 5 | OCA-B loss in CD4$^+$ T cells increases anergy in vitro. a, Naïve CD4$^+$ C57BL/6 T cells were stimulated in vitro for 24 hr with anti-CD3ε antibodies ± co-stimulation with CD28 antibodies. Lystates were prepared and subjected to immunoblotting using OCA-B antibodies. β-actin is shown as a loading control. **b**, Naïve OCA-B deficient and control CD4$^+$ T cells were stimulated in vitro with anti-CD3ε antibodies. 48 hr later, the cells were re-stimulated with PMA and ionomycin, and analyzed by flow cytometry. Representative frequencies of cytokine expressing CD4$^+$ CD44$^+$ cells are shown. **c**, Quantitation using independently purified cells from the spleens of 4 mice treated similar to (b). **d**, OCA-B deficient and control CD4$^+$ T cells were stimulated in vitro with indicated antibodies, and analyzed by flow cytometry. Mean of FR4^{hi} CD73^{hi} CD4$^+$ CD44$^+$ cell frequencies are shown using independently purified cells from the spleens of 3 mice, with two technical culture replicates performed for each mouse (n=6). **e**, Similar to panel (d), except frequencies of CD4$^+$CD44$^+$ICOS$^+$ cells are plotted. **f**, Similar to panel (d), except average percentage of CD4$^+$CD44$^+$CD25$^+$ cells are plotted.

Fig. 6 | Design and validation of OCA-B peptide inhibitors. a, OCA-B N-terminus/Oct1 DNA binding domain/octamer binding DNA co-crystal structure (PDB ID 1CQT)[48]. Gray: DNA. Green: Oct1 DNA binding domain. Cyan: OCA-B. Structured OCA-B N- and C-termini (residues 16 and 38) are labeled. Relevant OCA-B residues from panel (b) are highlighted. Red dashed line shows position of the Oct1 linker domain. **b**, Top alignment of the human androgen receptor (AR) isoform transcript variant 1 (Sequence ID: ADD26780.1) co-activator interaction domain (residues 698-721) with full-length human Oct1 and OCA-B. The Oct1 linker domain and OCA-B N-terminus most resemble the area of AR that interacts with Jmjd1a. Green serines: putative ERK phospho-acceptor sites. Yellow: similar or identical amino acids. Asterisks: known human point mutations that block coactivator binding and cause androgen insensitivity syndrome in humans. Pairwise alignments were performed using the FASTA algorithm (https://embnet.vital-it.ch/software/LALIGN_form.html) and trimmed for the 3-way overlap. **c**, Alignment of human and mouse primary OCA-B peptide sequences. **d**, Co-IP of Jmjd1a with double point-mutant OCA-B and wild-type control. HCT116 cells (which lack endogenous OCA-B) transfected with WT or mutant OCA-B constructs were used. Expression of

bioRxiv preprint doi: https://doi.org/10.1101/2020.02.06.937839; this version posted March 14, 2020. The copyright holder for this preprint (which was not certified by peer review) is the author/funder. All rights reserved. No reuse allowed without permission.

proteins was checked 48 hrs after transfection by Western blotting. 50 μg protein was loaded in each lane. **e**, Indicated peptide sequences were synthesized as C-terminal Tat fusions for membrane permeability. Arrows indicate position of mutant in (b) and (d). **f**, *Il2* mRNA expression in primary $CD4^+$ T cells treated with 50 μM JumOCA peptide was measured relative to β-actin internal standard by RT-qPCR. Cells were stimulated with CD3ε/CD28 antibodies for two days, rested for a further 8 days in the presence of exogenous recombinant IL-2, and restimulated for a further 6 hr. Peptide was included during resting and restimulation only, and replaced every other day with media changes. **g**, IL-2 cytokine expression in primary $CD4^+$ T cells cultured with 50μM peptide at initial treatment, and with 25μM peptide from the secondary treatment was measured by flow cytometry. Cells were treated similarly to (f) except collection, brefeldin A treatment and processing for flow cytometry occurred 24 hr post-restimulation. **h**, $CD4^+CD44^+IL2^+$ T cell frequencies from representative samples in panel (g) are shown. Plots were gated on CD4 and CD44. **i**, The interaction between OCA-B and Jmjd1a was measured in a co-immunoprecipitation assay. After incubation with protein-G beads, 0.2 μg/μL control scambled (Scram) or double point mutant (DM) peptide, or JumOCA peptide, were added for a further 3 hr prior to precipitation and washing. 1% input (lane 1) is shown as a control.

Fig. 7 | OCA-B inhibitor peptide injections protect NOD mice from newly-arisen diabetes. a, 3 doses of 10 mg/kg OCA-B inhibitor peptide (n=4) or control peptide (n=5) were injected retro-orbitally every 12 hr into 12-18 week-old NOD female littermate mice whose glucose levels were newly-risen above 225 mg/dL but still below 275 mg/dL. Glucose levels of peptide injected mice are shown right before each injection, and 12 hr after final injection. Control peptide=Tat alone. **b**, 4hr after the last injection of peptides in panel (a), PLN $CD4^+$ and $CD8^+$ T cell percentages were analyzed by flow cytometry. **c**, Mean of islet IL-17 expressing T cells in the same mice as in (b) were analyzed by flow cytometry and plotted. **d**, Similar analysis as (c) except for IFNγ.

bioRxiv preprint doi: https://doi.org/10.1101/2020.02.06.937839; this version posted March 14, 2020. The copyright holder for this preprint (which was not certified by peer review) is the author/funder. All rights reserved. No reuse allowed without permission.

References

1. Lernmark, A. & Larsson, H.E. Immune therapy in type 1 diabetes mellitus. *Nat Rev Endocrinol* **9**, 92-103 (2013).
2. Cooke, D.W. & Plotnick, L. Type 1 diabetes mellitus in pediatrics. *Pediatr Rev* **29**, 374-384; quiz 385 (2008).
3. Staeva, T.P., Chatenoud, L., Insel, R. & Atkinson, M.A. Recent lessons learned from prevention and recent-onset type 1 diabetes immunotherapy trials. *Diabetes* **62**, 9-17 (2013).
4. Shakya, A. *et al.* Oct1 and OCA-B are selectively required for CD4 memory T cell function. *J Exp Med* **212**, 2115-2131 (2015).
5. Kim, H. *et al.* T cell-selective deletion of Oct1 protects animals from autoimmune neuroinflammation while maintaining neurotropic pathogen response. *J Neuroinflammation* **16**, 133 (2019).
6. Shakya, A., Kang, J., Chumley, J., Williams, M.A. & Tantin, D. Oct1 is a switchable, bipotential stabilizer of repressed and inducible transcriptional states. *The Journal of biological chemistry* **286**, 450-459 (2011).
7. Yosef, N. *et al.* Dynamic regulatory network controlling TH17 cell differentiation. *Nature* **496**, 461-468 (2013).
8. van Heel, D.A. *et al.* Inflammatory bowel disease is associated with a TNF polymorphism that affects an interaction between the OCT1 and NF(-kappa)B transcription factors. *Hum Mol Genet* **11**, 1281-1289 (2002).
9. Vince, N. *et al.* HLA-C Level Is Regulated by a Polymorphic Oct1 Binding Site in the HLA-C Promoter Region. *Am J Hum Genet* **99**, 1353-1358 (2016).
10. Cunninghame Graham, D.S., Wong, A.K., McHugh, N.J., Whittaker, J.C. & Vyse, T.J. Evidence for unique association signals in SLE at the CD28-CTLA4-ICOS locus in a family-based study. *Hum Mol Genet* **15**, 3195-3205 (2006).
11. Kiesler, P., Shakya, A., Tantin, D. & Vercelli, D. An allergy-associated polymorphism in a novel regulatory element enhances IL13 expression. *Hum Mol Genet* **18**, 4513-4520 (2009).
12. Farh, K.K. *et al.* Genetic and epigenetic fine mapping of causal autoimmune disease variants. *Nature* **518**, 337-343 (2015).
13. Maurano, M.T. *et al.* Systematic localization of common disease-associated variation in regulatory DNA. *Science* **337**, 1190-1195 (2012).
14. Leon Rodriguez, D.A., Carmona, F.D., Echeverria, L.E., Gonzalez, C.I. & Martin, J. IL18 Gene Variants Influence the Susceptibility to Chagas Disease. *PLoS Negl Trop Dis* **10**, e0004583 (2016).
15. Games Collaborative, G. *et al.* Linkage disequilibrium screening for multiple sclerosis implicates JAG1 and POU2AF1 as susceptibility genes in Europeans. *J Neuroimmunol* **179**, 108-116 (2006).
16. Nakamura, M. *et al.* Genome-wide association study identifies TNFSF15 and POU2AF1 as susceptibility loci for primary biliary cirrhosis in the Japanese population. *Am J Hum Genet* **91**, 721-728 (2012).
17. Serreze, D.V. *et al.* B lymphocytes are essential for the initiation of T cell-mediated autoimmune diabetes: analysis of a new "speed congenic" stock of NOD.Ig mu null mice. *J Exp Med* **184**, 2049-2053 (1996).
18. Hattori, M. *et al.* The NOD mouse: recessive diabetogenic gene in the major histocompatibility complex. *Science* **231**, 733-735 (1986).

bioRxiv preprint doi: https://doi.org/10.1101/2020.02.06.937839; this version posted March 14, 2020. The copyright holder for this preprint (which was not certified by peer review) is the author/funder. All rights reserved. No reuse allowed without permission.

19. Serreze, D.V. *et al.* Subcongenic analysis of the Idd13 locus in NOD/Lt mice: evidence for several susceptibility genes including a possible diabetogenic role for beta 2-microglobulin. *J Immunol* **160**, 1472-1478 (1998).

20. Kim, U. *et al.* The B-cell-specific transcription coactivator OCA-B/OBF-1/Bob-1 is essential for normal production of immunoglobulin isotypes. *Nature* **383**, 542-547 (1996).

21. Wong, C.P., Li, L., Frelinger, J.A. & Tisch, R. Early autoimmune destruction of islet grafts is associated with a restricted repertoire of IGRP-specific CD8+ T cells in diabetic nonobese diabetic mice. *J Immunol* **176**, 1637-1644 (2006).

22. Makino, S., Muraoka, Y., Kishimoto, Y. & Hayashi, Y. Genetic analysis for insulitis in NOD mice. *Jikken Dobutsu* **34**, 425-431 (1985).

23. Rosmalen, J.G. *et al.* Subsets of macrophages and dendritic cells in nonobese diabetic mouse pancreatic inflammatory infiltrates: correlation with the development of diabetes. *Lab Invest* **80**, 23-30 (2000).

24. Peterson, J.D., Berg, R., Piganelli, J.D., Poulin, M. & Haskins, K. Analysis of leukocytes recruited to the pancreas by diabetogenic T cell clones. *Cell Immunol* **189**, 92-98 (1998).

25. Cantor, J. & Haskins, K. Recruitment and activation of macrophages by pathogenic CD4 T cells in type 1 diabetes: evidence for involvement of CCR8 and CCL1. *J Immunol* **179**, 5760-5767 (2007).

26. Schloot, N.C. *et al.* Serum IFN-gamma and IL-10 levels are associated with disease progression in non-obese diabetic mice. *Diabetes Metab Res Rev* **18**, 64-70 (2002).

27. Newby, B.N. *et al.* Type 1 Interferons Potentiate Human CD8(+) T-Cell Cytotoxicity Through a STAT4- and Granzyme B-Dependent Pathway. *Diabetes* **66**, 3061-3071 (2017).

28. Krishnamurthy, B. *et al.* Autoimmunity to both proinsulin and IGRP is required for diabetes in nonobese diabetic 8.3 TCR transgenic mice. *J Immunol* **180**, 4458-4464 (2008).

29. Wang, B. *et al.* Interferon-gamma impacts at multiple points during the progression of autoimmune diabetes. *Proc Natl Acad Sci U S A* **94**, 13844-13849 (1997).

30. Brode, S., Raine, T., Zaccone, P. & Cooke, A. Cyclophosphamide-induced type-1 diabetes in the NOD mouse is associated with a reduction of CD4+CD25+Foxp3+ regulatory T cells. *J Immunol* **177**, 6603-6612 (2006).

31. Jaeckel, E., von Boehmer, H. & Manns, M.P. Antigen-specific FoxP3-transduced T-cells can control established type 1 diabetes. *Diabetes* **54**, 306-310 (2005).

32. Mellanby, R.J., Thomas, D., Phillips, J.M. & Cooke, A. Diabetes in non-obese diabetic mice is not associated with quantitative changes in CD4+ CD25+ Foxp3+ regulatory T cells. *Immunology* **121**, 15-28 (2007).

33. Li, L. *et al.* beta cell-specific CD4+ T cell clonotypes in peripheral blood and the pancreatic islets are distinct. *J Immunol* **183**, 7585-7591 (2009).

34. Berry, G. & Waldner, H. Accelerated type 1 diabetes induction in mice by adoptive transfer of diabetogenic CD4+ T cells. *J Vis Exp*, e50389 (2013).

35. Presa, M. *et al.* The Presence and Preferential Activation of Regulatory T Cells Diminish Adoptive Transfer of Autoimmune Diabetes by Polyclonal Nonobese Diabetic (NOD) T Cell Effectors into NSG versus NOD-scid Mice. *J Immunol* **195**, 3011-3019 (2015).

36. Van Belle, T.L., Taylor, P. & von Herrath, M.G. Mouse Models for Type 1 Diabetes. *Drug Discov Today Dis Models* **6**, 41-45 (2009).

bioRxiv preprint doi: https://doi.org/10.1101/2020.02.06.937839; this version posted March 14, 2020. The copyright holder for this preprint (which was not certified by peer review) is the author/funder. All rights reserved. No reuse allowed without permission.

37. Kurts, C. *et al.* CD4+ T cell help impairs CD8+ T cell deletion induced by cross-presentation of self-antigens and favors autoimmunity. *J Exp Med* **186**, 2057-2062 (1997).

38. Verdaguer, J. *et al.* Spontaneous autoimmune diabetes in monoclonal T cell nonobese diabetic mice. *J Exp Med* **186**, 1663-1676 (1997).

39. Kalekar, L.A. *et al.* CD4(+) T cell anergy prevents autoimmunity and generates regulatory T cell precursors. *Nat Immunol* **17**, 304-314 (2016).

40. Vanasek, T.L., Khoruts, A., Zell, T. & Mueller, D.L. Antagonistic roles for CTLA-4 and the mammalian target of rapamycin in the regulation of clonal anergy: enhanced cell cycle progression promotes recall antigen responsiveness. *J Immunol* **167**, 5636-5644 (2001).

41. Kearney, E.R., Pape, K.A., Loh, D.Y. & Jenkins, M.K. Visualization of peptide-specific T cell immunity and peripheral tolerance induction in vivo. *Immunity* **1**, 327-339 (1994).

42. Chai, J.G. & Lechler, R.I. Immobilized anti-CD3 mAb induces anergy in murine naive and memory CD4+ T cells in vitro. *Int Immunol* **9**, 935-944 (1997).

43. Tuettenberg, A. *et al.* The role of ICOS in directing T cell responses: ICOS-dependent induction of T cell anergy by tolerogenic dendritic cells. *J Immunol* **182**, 3349-3356 (2009).

44. Dong, C. & Nurieva, R.I. Regulation of immune and autoimmune responses by ICOS. *J Autoimmun* **21**, 255-260 (2003).

45. Dong, C. *et al.* ICOS co-stimulatory receptor is essential for T-cell activation and function. *Nature* **409**, 97-101 (2001).

46. Martinez, R.J. *et al.* Arthritogenic self-reactive CD4+ T cells acquire an FR4hiCD73hi anergic state in the presence of Foxp3+ regulatory T cells. *J Immunol* **188**, 170-181 (2012).

47. Skwarczynska, M. & Ottmann, C. Protein-protein interactions as drug targets. *Future Med Chem* **7**, 2195-2219 (2015).

48. Green, D.R. A BH3 Mimetic for Killing Cancer Cells. *Cell* **165**, 1560 (2016).

49. Polo, J.M. *et al.* Specific peptide interference reveals BCL6 transcriptional and oncogenic mechanisms in B-cell lymphoma cells. *Nat Med* **10**, 1329-1335 (2004).

50. Chasman, D., Cepek, K., Sharp, P.A. & Pabo, C.O. Crystal structure of an OCA-B peptide bound to an Oct-1 POU domain/octamer DNA complex: specific recognition of a protein-DNA interface. *Genes Dev* **13**, 2650-2657 (1999).

51. Klemm, J.D., Rould, M.A., Aurora, R., Herr, W. & Pabo, C.O. Crystal structure of the Oct-1 POU domain bound to an octamer site: DNA recognition with tethered DNA-binding modules. *Cell* **77**, 21-32 (1994).

52. Gstaiger, M., Georgiev, O., van Leeuwen, H., van der Vliet, P. & Schaffner, W. The B cell coactivator Bob1 shows DNA sequence-dependent complex formation with Oct-1/Oct-2 factors, leading to differential promoter activation. *EMBO J* **15**, 2781-2790 (1996).

53. Yamane, K. *et al.* JHDM2A, a JmjC-containing H3K9 demethylase, facilitates transcription activation by androgen receptor. *Cell* **125**, 483-495 (2006).

54. Thin, T.H. *et al.* Mutations in the helix 3 region of the androgen receptor abrogate ARA70 promotion of 17beta-estradiol-induced androgen receptor transactivation. *The Journal of biological chemistry* **277**, 36499-36508 (2002).

55. Schwarze, S.R., Hruska, K.A. & Dowdy, S.F. Protein transduction: unrestricted delivery into all cells? *Trends Cell Biol* **10**, 290-295 (2000).

bioRxiv preprint doi: https://doi.org/10.1101/2020.02.06.937839; this version posted March 14, 2020. The copyright holder for this preprint (which was not certified by peer review) is the author/funder. All rights reserved. No reuse allowed without permission.

56. Caron, N.J., Quenneville, S.P. & Tremblay, J.P. Endosome disruption enhances the functional nuclear delivery of Tat-fusion proteins. *Biochem Biophys Res Commun* **319**, 12-20 (2004).

57. Krautwald, S., Ziegler, E., Tiede, K., Pust, R. & Kunzendorf, U. Transduction of the TAT-FLIP fusion protein results in transient resistance to Fas-induced apoptosis in vivo. *The Journal of biological chemistry* **279**, 44005-44011 (2004).

58. Shi, W. *et al.* Transcriptional profiling of mouse B cell terminal differentiation defines a signature for antibody-secreting plasma cells. *Nat Immunol* **16**, 663-673 (2015).

59. Kawakami, N. *et al.* Autoimmune CD4+ T cell memory: lifelong persistence of encephalitogenic T cell clones in healthy immune repertoires. *J Immunol* **175**, 69-81 (2005).

60. Yeo, L. *et al.* Autoreactive T effector memory differentiation mirrors beta cell function in type 1 diabetes. *J Clin Invest* **128**, 3460-3474 (2018).

61. Chee, J. *et al.* Effector-memory T cells develop in islets and report islet pathology in type 1 diabetes. *J Immunol* **192**, 572-580 (2014).

62. Parker, M.J. *et al.* Immune depletion with cellular mobilization imparts immunoregulation and reverses autoimmune diabetes in nonobese diabetic mice. *Diabetes* **58**, 2277-2284 (2009).

63. Ikegami, I., Takaki, H., Kamiya, S., Kamekura, R. & Ichimiya, S. Bob1 enhances RORgammat-mediated IL-17A expression in Th17cells through interaction with RORgammat. *Biochem Biophys Res Commun* **514**, 1167-1171 (2019).

64. Chevrier, S., Kratina, T., Emslie, D., Karnowski, A. & Corcoran, L.M. Germinal center-independent, IgM-mediated autoimmunity in sanroque mice lacking Obf1. *Immunol Cell Biol* **92**, 12-19 (2014).

65. Casellas, R. *et al.* OcaB is required for normal transcription and V(D)J recombination of a subset of immunoglobulin kappa genes. *Cell* **110**, 575-585 (2002).

66. Citro, A. *et al.* CXCR1/2 inhibition blocks and reverses type 1 diabetes in mice. *Diabetes* **64**, 1329-1340 (2015).

67. Diana, J. & Lehuen, A. Macrophages and beta-cells are responsible for CXCR2-mediated neutrophil infiltration of the pancreas during autoimmune diabetes. *EMBO Mol Med* **6**, 1090-1104 (2014).

68. Haskins, K. Pathogenic T-cell clones in autoimmune diabetes: more lessons from the NOD mouse. *Adv Immunol* **87**, 123-162 (2005).

69. Kurts, C. *et al.* Constitutive class I-restricted exogenous presentation of self antigens in vivo. *J Exp Med* **184**, 923-930 (1996).

70. Katz, J.D., Wang, B., Haskins, K., Benoist, C. & Mathis, D. Following a diabetogenic T cell from genesis through pathogenesis. *Cell* **74**, 1089-1100 (1993).

71. Delong, T. *et al.* Pathogenic CD4 T cells in type 1 diabetes recognize epitopes formed by peptide fusion. *Science* **351**, 711-714 (2016).

72. Zuber, J. *et al.* RNAi screen identifies Brd4 as a therapeutic target in acute myeloid leukaemia. *Nature* **478**, 524-528 (2011).

73. Zwilling, S., Dieckmann, A., Pfisterer, P., Angel, P. & Wirth, T. Inducible expression and phosphorylation of coactivator BOB.1/OBF.1 in T cells. *Science* **277**, 221-225 (1997).

74. Testa, G. *et al.* A reliable lacZ expression reporter cassette for multipurpose, knockout-first alleles. *Genesis* **38**, 151-158 (2004).

bioRxiv preprint doi: https://doi.org/10.1101/2020.02.06.937839; this version posted March 14, 2020. The copyright holder for this preprint (which was not certified by peer review) is the author/funder. All rights reserved. No reuse allowed without permission.

940 75. Sitrin, J., Ring, A., Garcia, K.C., Benoist, C. & Mathis, D. Regulatory T cells control NK cells in an
941 insulitic lesion by depriving them of IL-2. *J Exp Med* **210**, 1153-1165 (2013).

942 76. Gstaiger, M., Knoepfel, L., Georgiev, O., Schaffner, W. & Hovens, C.M. A B-cell coactivator of
943 octamer-binding transcription factors. *Nature* **373**, 360-362 (1995).

944 77. Zhang, C. *et al.* Elimination of insulitis and augmentation of islet beta cell regeneration via induction of
945 chimerism in overtly diabetic NOD mice. *Proc Natl Acad Sci U S A* **104**, 2337-2342 (2007).

946

947

bioRxiv preprint doi: https://doi.org/10.1101/2020.02.06.937839; this version posted March 14, 2020. The copyright holder for this preprint (which was not certified by peer review) is the author/funder. All rights reserved. No reuse allowed without permission.

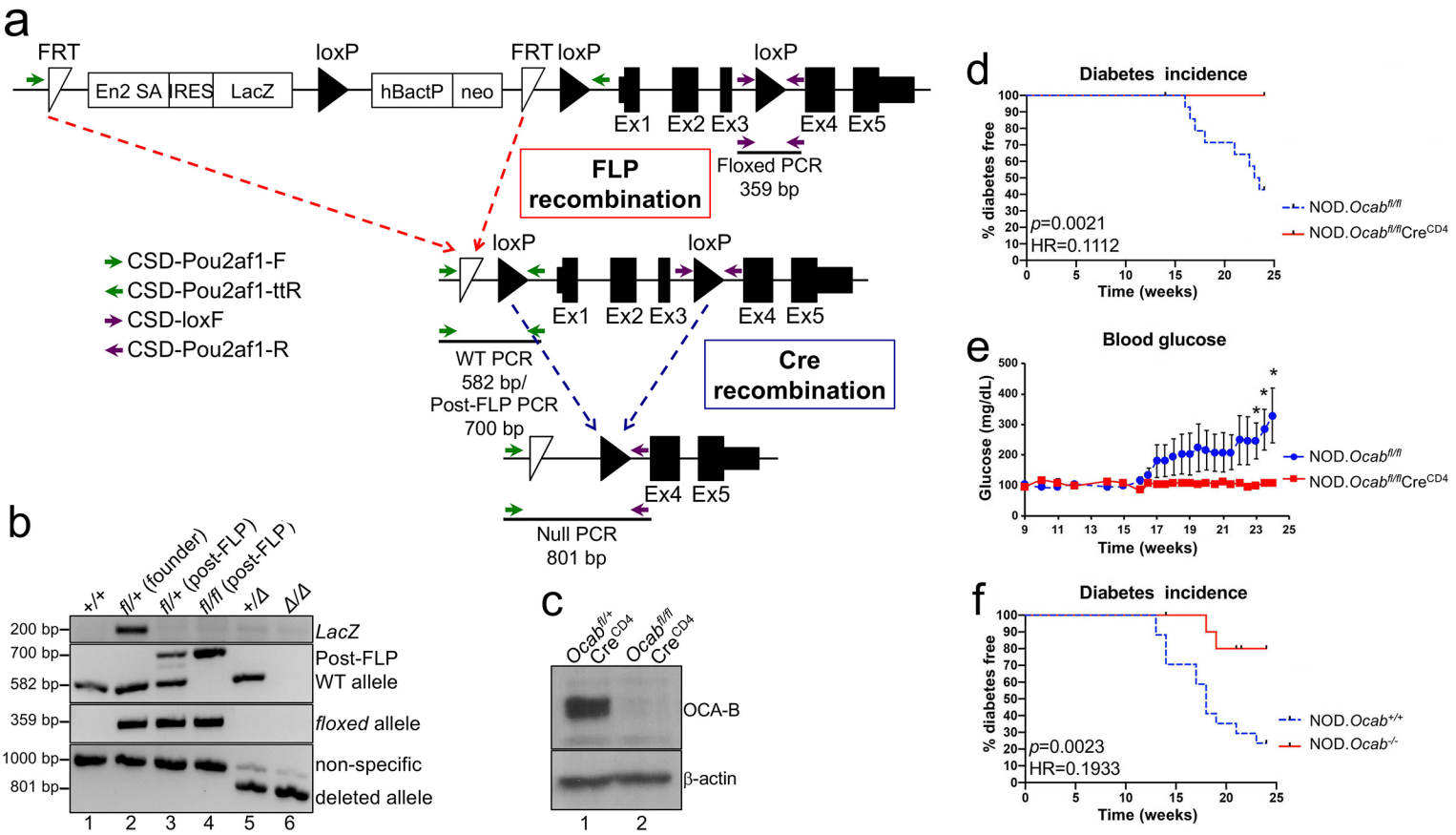

bioRxiv preprint doi: https://doi.org/10.1101/2020.02.06.937839; this version posted March 14, 2020. The copyright holder for this preprint (which was not certified by peer review) is the author/funder. All rights reserved. No reuse allowed without permission.

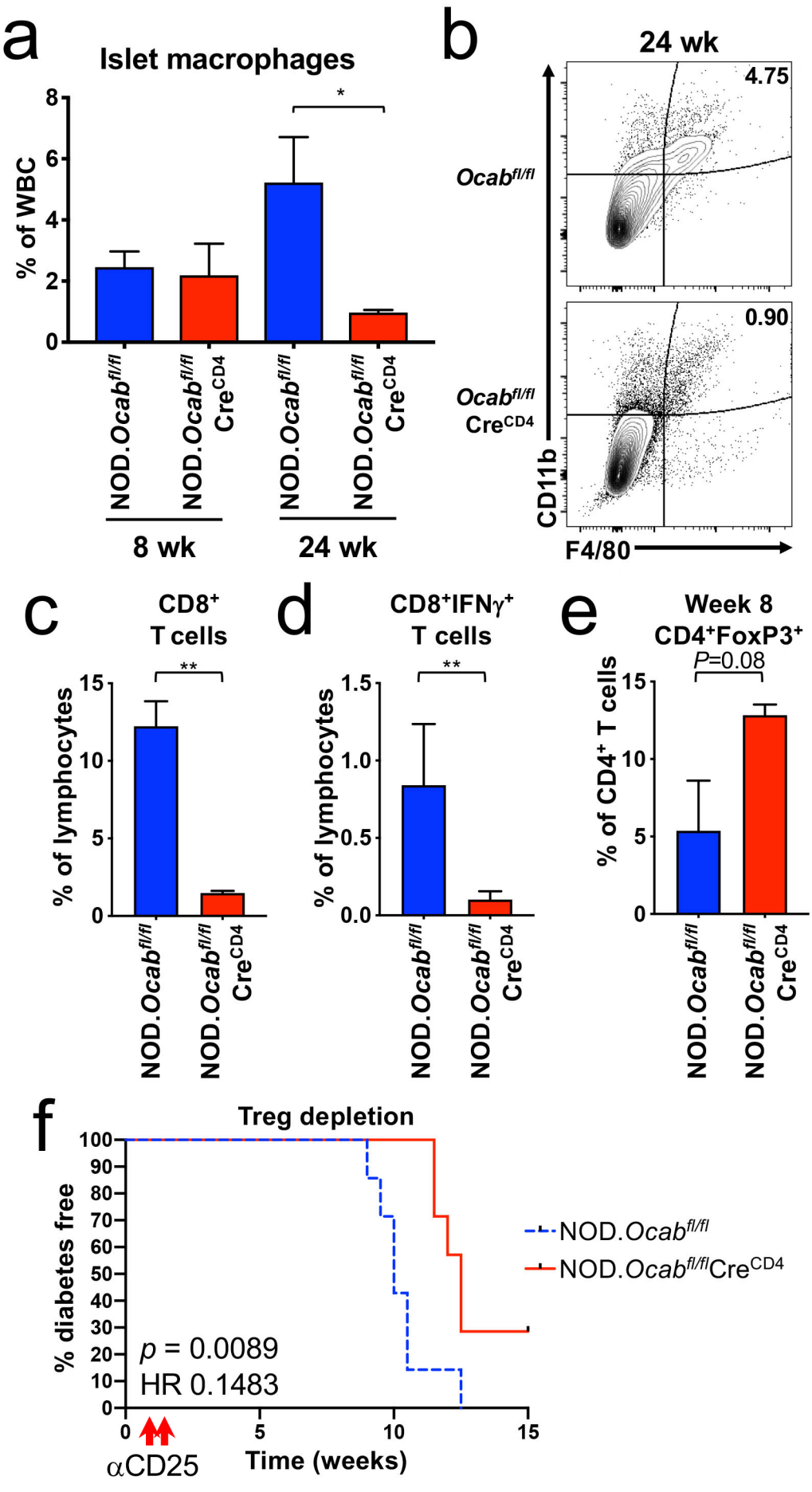

bioRxiv preprint doi: https://doi.org/10.1101/2020.02.06.937839; this version posted March 14, 2020. The copyright holder for this preprint (which was not certified by peer review) is the author/funder. All rights reserved. No reuse allowed without permission.

Kim et al. Figure 3

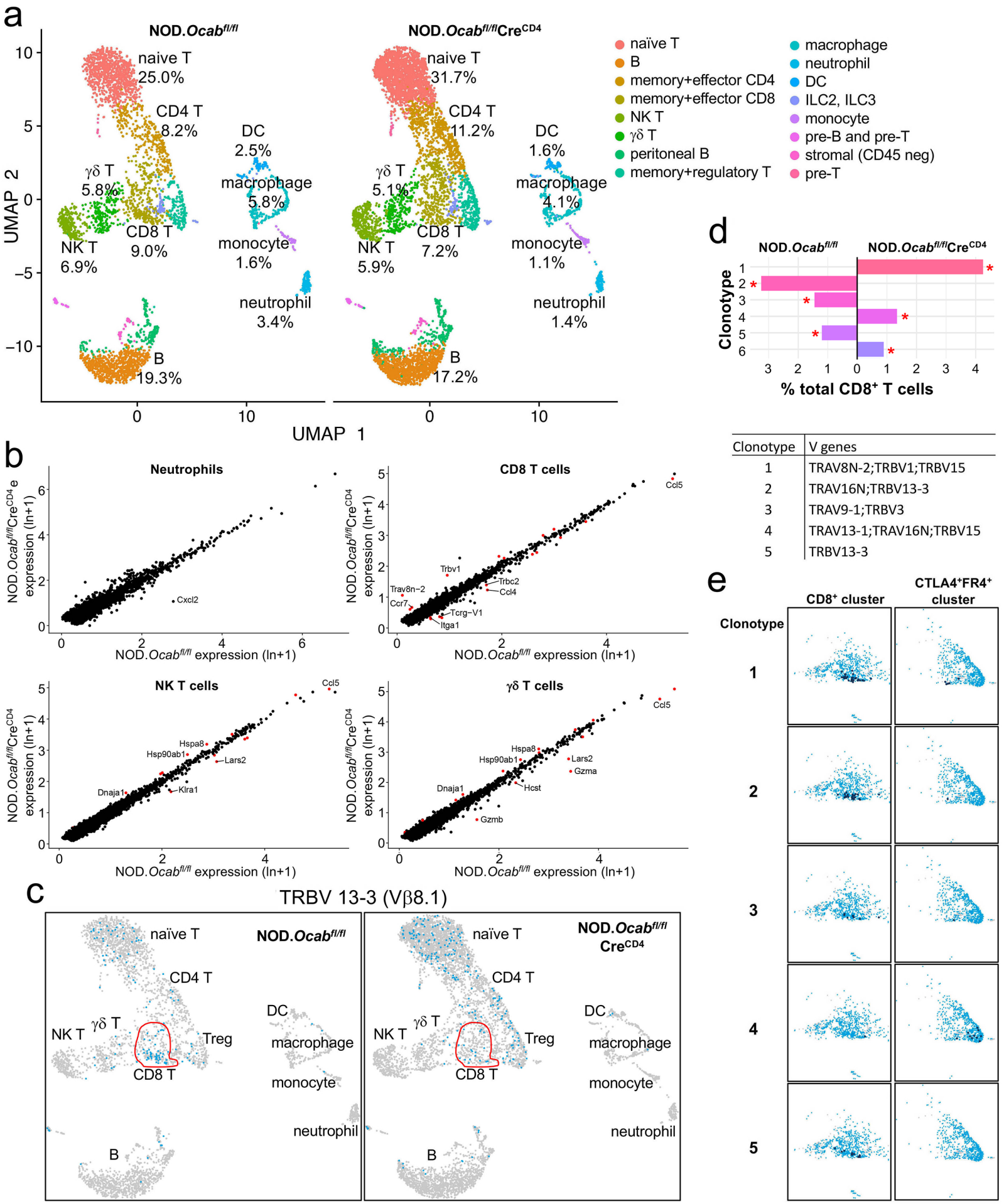

Clonotype	V genes
1	TRAV8N-2;TRBV1;TRBV15
2	TRAV16N;TRBV13-3
3	TRAV9-1;TRBV3
4	TRAV13-1;TRAV16N;TRBV15
5	TRBV13-3

bioRxiv preprint doi: https://doi.org/10.1101/2020.02.06.937839; this version posted March 14, 2020. The copyright holder for this preprint (which was not certified by peer review) is the author/funder. All rights reserved. No reuse allowed without permission.

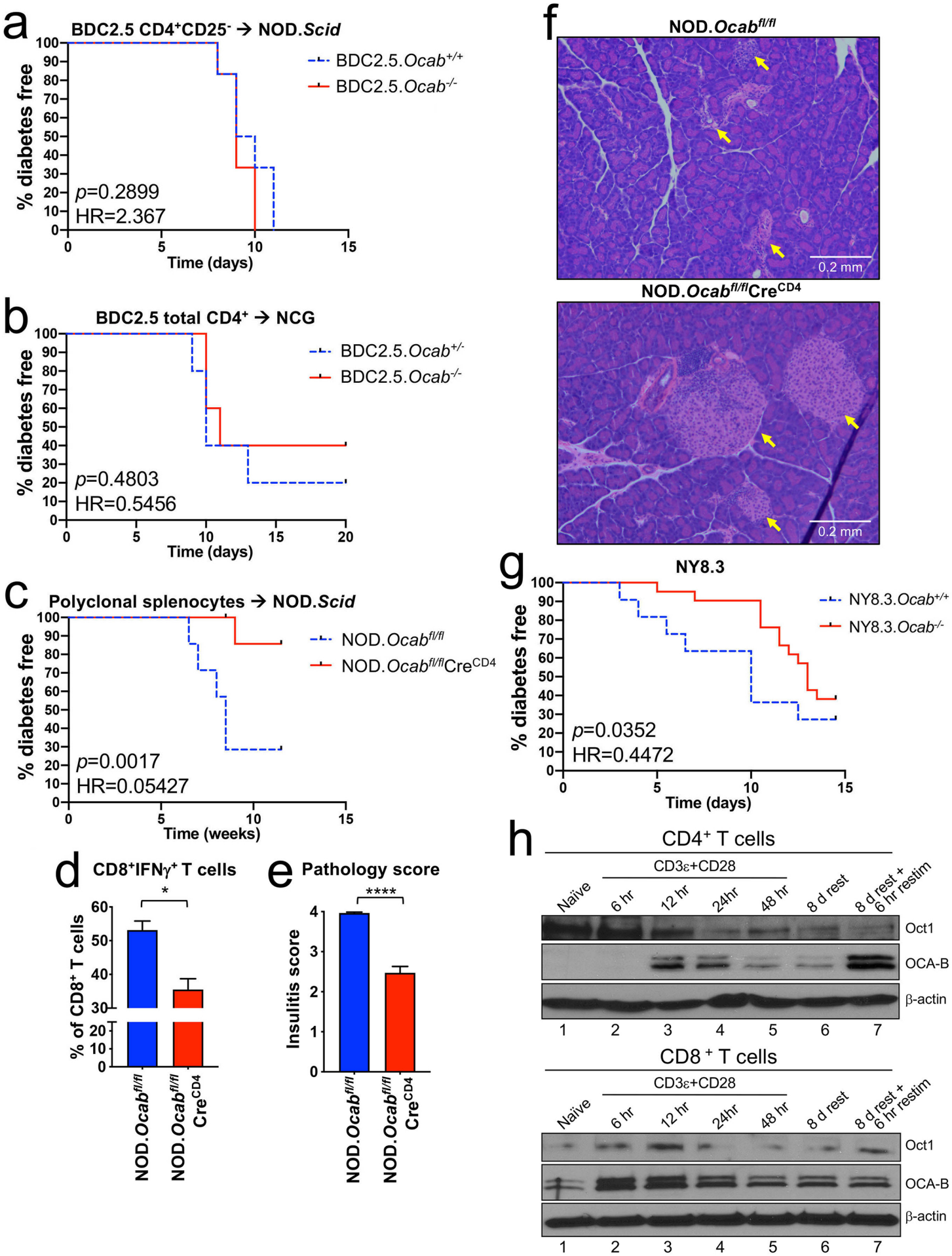

bioRxiv preprint doi: https://doi.org/10.1101/2020.02.06.937839; this version posted March 14, 2020. The copyright holder for this preprint (which was not certified by peer review) is the author/funder. All rights reserved. No reuse allowed without permission.

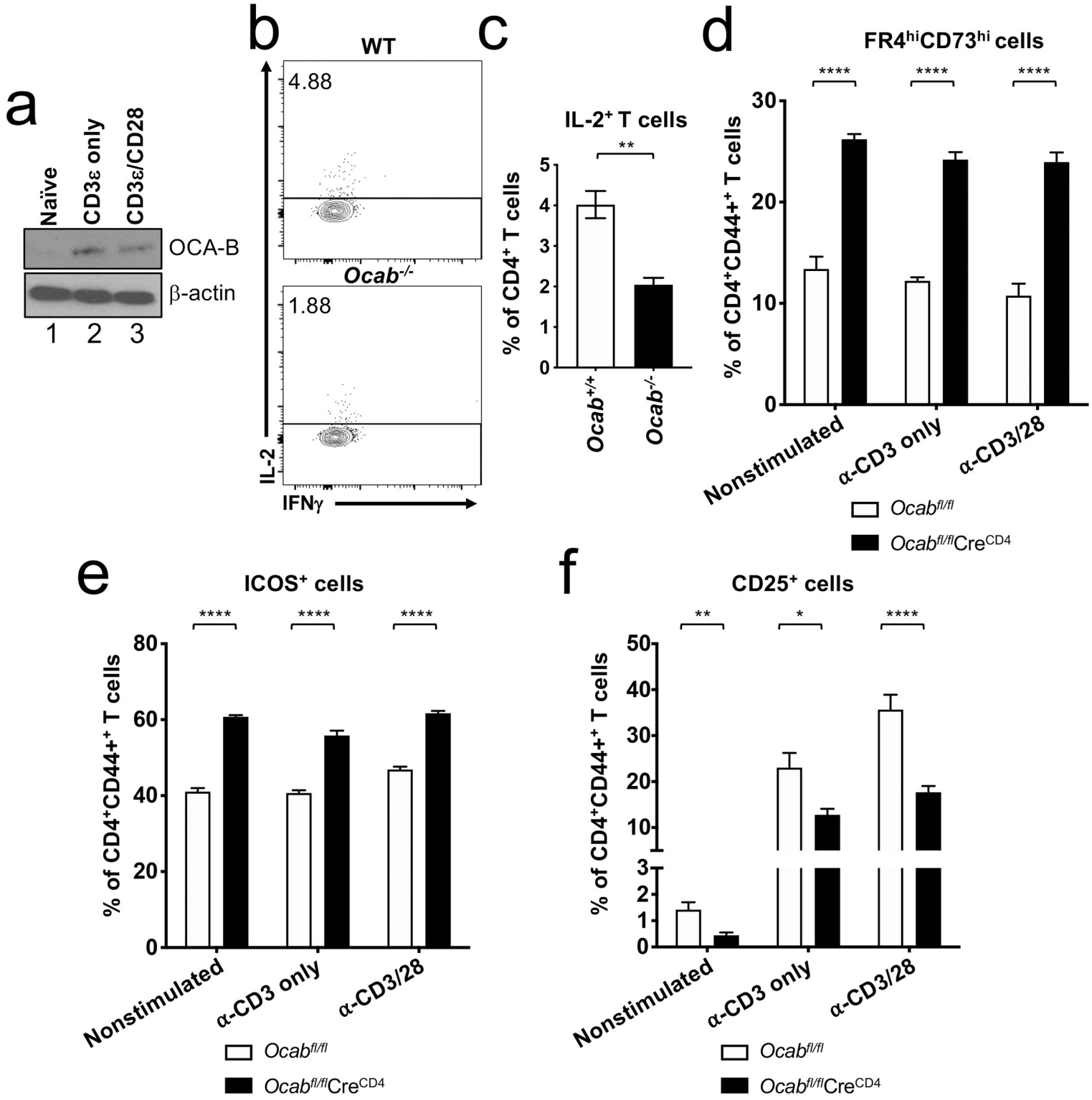

bioRxiv preprint doi: https://doi.org/10.1101/2020.02.06.937839; this version posted March 14, 2020. The copyright holder for this preprint (which was not certified by peer review) is the author/funder. All rights reserved. No reuse allowed without permission.

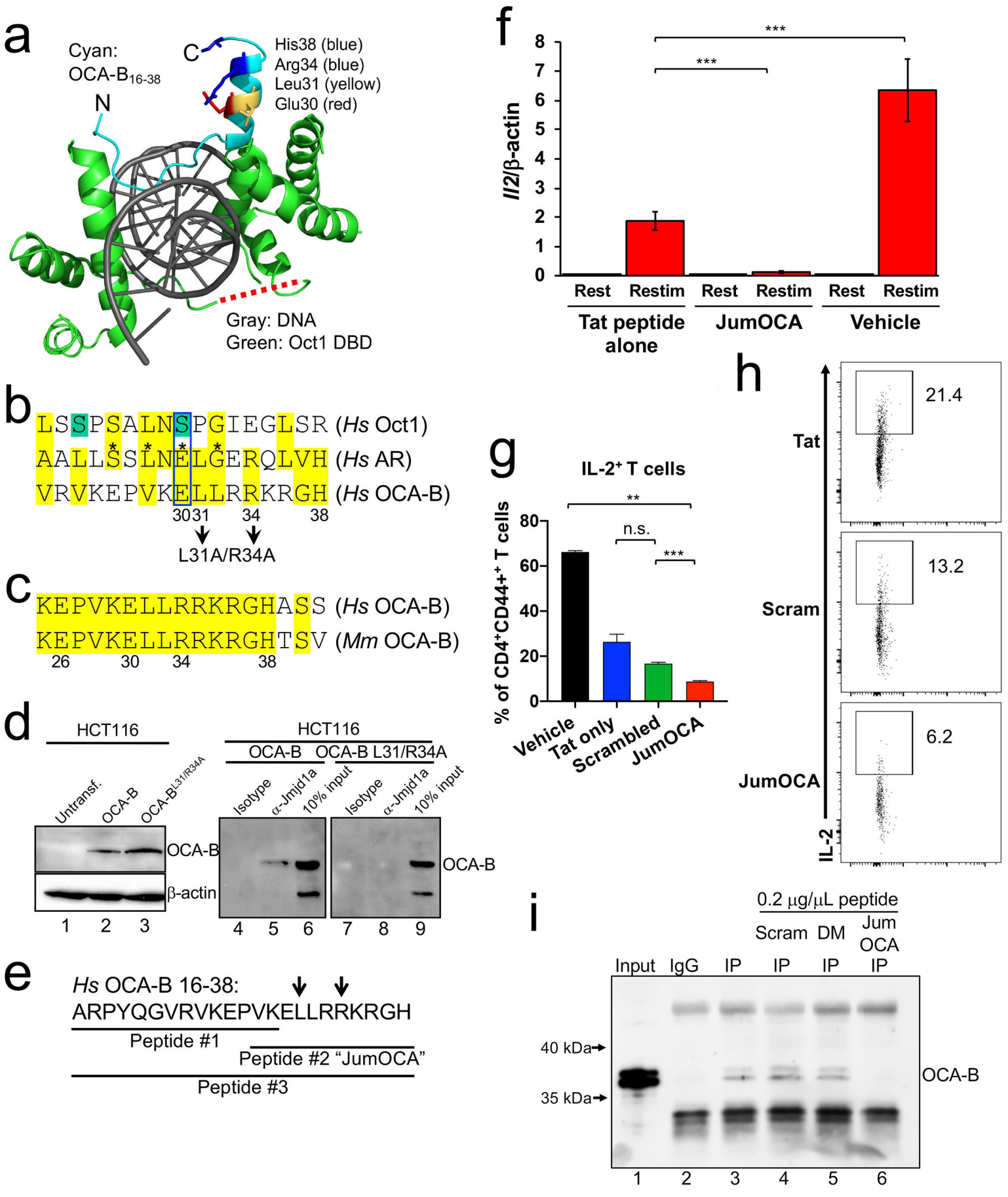

bioRxiv preprint doi: https://doi.org/10.1101/2020.02.06.937839; this version posted March 14, 2020. The copyright holder for this preprint (which was not certified by peer review) is the author/funder. All rights reserved. No reuse allowed without permission.